

5-2009

Electrochemically mediated charge transfer effects on single-walled carbon nanotubes.

Buddika KA. Abeyweera 1980-
University of Louisville

Follow this and additional works at: <https://ir.library.louisville.edu/etd>

 Part of the [Physics Commons](#)

Recommended Citation

Abeyweera, Buddika KA. 1980-, "Electrochemically mediated charge transfer effects on single-walled carbon nanotubes." (2009).
Electronic Theses and Dissertations. Paper 8.
<https://doi.org/10.18297/etd/8>

This Master's Thesis is brought to you for free and open access by ThinkIR: The University of Louisville's Institutional Repository. It has been accepted for inclusion in Electronic Theses and Dissertations by an authorized administrator of ThinkIR: The University of Louisville's Institutional Repository. This title appears here courtesy of the author, who has retained all other copyrights. For more information, please contact thinkir@louisville.edu.

**ELECTROCHEMICALLY MEDIATED CHARGE TRANSFER
EFFECTS ON SINGLE-WALLED CARBON NANOTUBES**

By

Buddika K.A. Abeyweera MP
BSc. (Physics Hons.) University of Peradeniya, Sri Lanka

A Thesis
Submitted to the Faculty of the
Graduate School of the University of Louisville
In Partial Fulfillment of the Requirements
For the Degree of

Master of Science

Department of Physics
University of Louisville
Louisville, Kentucky

May 2009

**ELECTROCHEMICALLY MEDIATED CHARGE TRANSFER
EFFECTS ON SINGLE-WALLED CARBON NANOTUBES**

By

Buddika KA Abeyweera MP
BSc.(Physics Hons.) University of Peradeniya, Sri Lanka 2006

A Thesis Approved on

April 9, 2009

by the Following Thesis Committee:

Dr. Gamini Sumanasekara (Thesis Director)

Dr. Shi Yu Wu

Dr.Cindy Harnett

ACKNOWLEDGEMENTS

I would like to thank my thesis advisor Dr. Gamini Sumanasekara for his untiring support and contributions towards my research. It would not have been possible without his guidance and encouragement. Thank you for patiently sharing all the knowledge.

I would like to thank my committee members Dr. Shi Y. Wu and Dr. C. Harnett for the guidance and being in my thesis committee and I would also like to thank my lab colleagues for their support. Specially, I would like to express my gratitude to Dr. Sharvil Desai for his valuable time in helping me with experimental equipment. Also many thanks go to Dr. William Martin and other lab mates for making the lab experience educational and enjoyable.

Finally I would like to thank my parents for their endless love and support throughout these years. At last but not least many thanks to my wife Piyumika Suriyampola for her great patience, love and endless support for making this success. This will not be possible without her great encouragement in my ups and downs.

ABSTRACT

ELECTROCHEMICALLY MEDIATED CHARGE TRANSFER EFFECTS ON SINGLE-WALLED CARBON NANOTUBES

Buddika KA Abeyweera MP

09th of May 2009

This thesis is based on experimental work on electrochemically mediated charge transfer effects on Single-walled carbon nanotube bundles. The study of these effects are very important towards understanding the sensitivity of gases on nanostructures like single-walled carbon nanotubes. Chapter one covers the introduction and overview of carbon nanostructures including single-walled carbon nanotubes. Chapter two covers the experimental techniques involving sample preparation, experimental setup and data acquisition. Chapter three consists of Results and the Discussions explaining the mechanisms based on charge transfer mechanism. In the final chapter, implications and the importance of the study are explained.

Single-walled carbon nanotubes are used as chemical gas sensors due to its high sensitivity and rapid response to various gases. Studying the electrical properties of single-walled carbon nanotubes increased the interest for further study related to sensor properties. Intrinsic properties of SWNT thin films have been studied extensively by measuring *in situ* thermoelectric power and 4 probe resistances. Recently, it has been

shown that the conductivity and the type of SWNT material change dramatically due to exposure of SWNT sample to various gases. Even though several mechanisms have been proposed to explain this phenomenon, it has been a controversial since the presence of water vapor barrier is not taken into consideration for explaining the mechanism. Electrochemically mediated charge transfer has been studied by its effects on the surface conductivity of diamond. And It has been shown that a pronounced conductivity been observed in Hydrogen terminated diamond even though it shows an insulating properties. We proposed a mechanism for the change of intrinsic properties of semiconducting SWNTs by systematically shifting the Fermi energy level by the exposure of different pH saturated water vapors. Due to the change in chemical potential of the redox couple of various gas saturated water vapor and Fermi energy of SWNT will result in charge transfer from water layer to SWNT or vice versa. The changes in thermoelectric power and Resistance data correlate with relative position of the Fermi level with respect to the chemical potential of the aqueous layer. SWNT samples were prepared by Pulse Laser Vaporization technique and purified by standard chemical methods. Experiments were performed using ambient oxygen and ammonia which have been bubbled through acid and basic solutions of different pH values at atmospheric pressure and room temperature.

TABLE OF CONTENTS

	PAGE
ACKNOWLEDGEMENTS.....	iii
ABSTRACT.....	iv
LIST OF FIGURES.....	viii
CHAPTER	
I. INTRODUCTION	1
Nanoscience & Nanotechnology.....	1
An Introduction to Single-walled carbon Nanotubes.....	2
Band Structure and Density of States of SWNTs.....	6
Synthesize of Carbon nanotubes.....	10
Purification.....	8
Characterization Techniques.....	19
Applications of Nanotubes.....	27
Thermoelectric power of Metals and Semiconductors.....	31
II. EXPERIMENTAL TECHNIQUES.....	34
Preparation of thin films of SWCNTs.....	34
Experimental Setup.....	35
Experimental Procedure.....	39

III. RESULTS & DISCUSSION.....	41
Chemical Potential & pH values of Aqueous solutions.....	44
TEP & Resistance measurements on Electrochemical charge transfer between the SWCNT thin film and the aqueous solutions.....	47
IV. CONCLUSIONS.....	57
REFERENCES	58
CURRICULUM VITAE.....	60

LIST OF FIGURES

FIGURE	PAGE
1. Creation of SWNT by rolling-up of a 2-D graphene sheet.....	2
2. The unrolled honey comb lattice which shows the chiral vector.....	3
3. Classification of SWNTs.....	4
4. Atomically resolved STM images of individual SWNTs.....	4
5. The Conduction & Valence band line-up for metallic and semiconducting nanotubes.....	6
6. Direct & Reciprocal lattice structures of a 2-D graphene sheet	7
7. Energy band diagram of a 2-D graphene sheet.....	9
8. Energy dispersion curves for armchair, zigzag & chiral nanotubes.....	10
9. Density of States of metallic & semiconducting nanotubes.....	11
10. Reactor used to produce SWNTs using Laser ablation technique.....	13
11. The diagram of an Electric Arc Reactor.....	15
12. Schematic diagram of a CVD Reactor.....	17
13. The Electron ray and the diffraction pattern diagram of a TEM.....	21
14. A schematic diagram of a basic components of a SEM.....	23
15. Raman spectrum of SWNT bundle, metallic & SC isolated SWNTs.....	26
16. Schematic diagram of a microfabricated FET using a SWNT.....	30
17. The change in conductance due to exposure of NO ₂ & NH ₃ gases.....	31

18. The sample with the probe.....	36
19. Schematic diagram of the Analogue subtraction circuit.....	37
20. Figure of Analogue subtraction circuit.....	38
21. The Experimental Setup.....	39
22. The Glass setup used to introduce pH solutions.....	39
23. The user interface labview program used to collect TEP data for the thin film sample.....	41
24. HRSEM images of SWNT sample.....	42
25. The Raman spectrum of the sample.....	43
26. Optical Absorptance of the SWNT film obtained by UV-VISIBLE-NIR spectrometer.....	44
27. Curve fitting of the UV-VISIBLE-NIR spectrum.....	45
28. Graph of CP as a function of pH value at partial pressure of 1bar of oxygen.....	46
29. Graph of CP as a function of partial pressure of oxygen at pH1.68.....	47
30. N-type Conductivity of the sample under vacuum.....	48
31. The Thermopower data of exposure to oxygen through different pH values.....	49
32. The graph of Resistance against time for oxygen exposure to different pH values.....	50
33. The graphs of TEP and Resistance plotted against time for exposure of oxygen gas through acidic solution.....	51
34. The Band line-up diagram for charge transfer between SWNT sample and an acidic solution.....	52
35. The graphs of TEP and Resistance plotted against time for exposure of oxygen gas through basic solution.....	53
36. The Band line-up diagram for charge transfer between SWNT sample and a basic solution.....	54

37. Graph of Thermoelectric power against time for hydrous ammonia.....55

CHAPTER 1: INTRODUCTION

Nanoscience and Nanotechnology

Nanotechnology has recently received extensive attention through out the technical world due to their dimensions and outstanding material properties. The physical variations of synthesized nanomaterials such as the diameter lead to a striking changes in their electrical, optical, chemical, biological, electro-optical and magnetic properties. Due to these phenomenal behaviors of nanomaterials, Nanoscience and Nanotechnology have invaded every part of today's world by its applications. Nanotechnology which is driven by nanomaterials can be classified into two parts namely nanostructured materials and nanophase materials depending on their structures. Nanophase materials are basically nanoparticles and catalysts in which nanoparticles can be ceramics, composite materials, polymeric materials or even metals. These are importantly used in nanoelectronic industry as insulating matrices. On the other hand nanostructured materials such as nanowires, nanoweb, nanotubes and thin films are widely used in all industries due to their remarkable electrical and mechanical properties. Out of these nanomaterials, carbon nanotubes are considered as the major ingredient in nanoscience because of its unique physical and electrical properties. The tensile strength and stiffness of the carbon nanotubes are about hundred times that of steel and the electrical conductivity is similar to that of steel which is desired by many electrical applications. Further more, thermal

conductivity of carbon nanotubes is somewhat similar to diamond. Although many scientists have contributed to the discovery of carbon nanotubes, the report of Sumio Iijima of NEC in 1991 is of particular importance because it put carbon nanotubes at the spotlight of the scientific community.

An Introduction to Single-walled carbon nanotubes

A single-walled carbon nanotube can be geometrically considered as a single graphene sheet wrapping up to form a seamless tube which has a length of thousand times of the tube diameter. Thus, a SWNT enclose a hollow cylindrical pore. The most common starting materials used to make SWNT are graphite, which consists of graphene sheets of a 2-D honey-comb structure as shown in Figure 1.

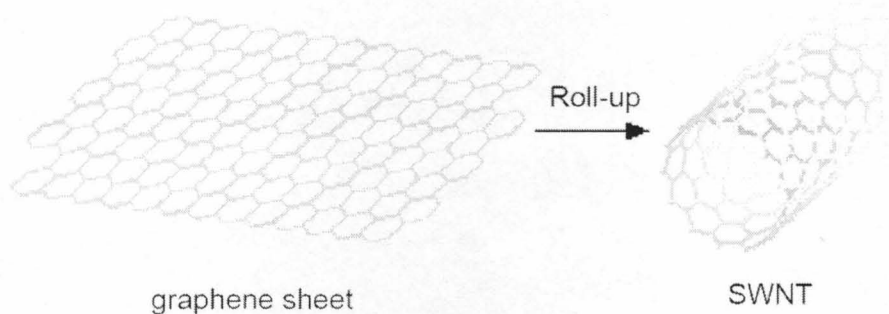


Fig 1: Creation of SWNT by rolling-up of a 2-D graphene sheet.

Carbon nanotubes appear as single hollow cylinders which of course called as single-walled carbon nanotubes (SWNT) as well as two concentric cylinders which are called double-walled carbon nanotubes (DWNT). Multi-walled carbon nanotubes come up with multiple concentric cylinders (MWNT). The diameter of a single-walled carbon nanotube is in the range of 0.7nm-10nm, but most of them are less than 2nm. Single-walled carbon

nanotubes are the basic structures of creating double-walled and multi-walled carbon nanotubes which they have some unique properties which are not shown by double-walled or multi-walled nanotubes. Generally, carbon nanotubes can be classified into two categories due to their structure's symmetry namely chiral(non-Symmorphic) and achiral(Symmorphic). Symmorphic nanotubes can be further divided into two classes such as armchair and zigzag. So we can say that there are three types of nanotubes classified by the way the 2-D graphene sheet is rolled-up. The lattice structure of a SWNT can be viewed by how the graphene sheet is wrapped into the nanotube and it is represented by a pair of indices (n,m) which is called chiral vector (C_h)[1].

$$C_h = na_1 + ma_2 \quad (0 \leq m \leq n)$$

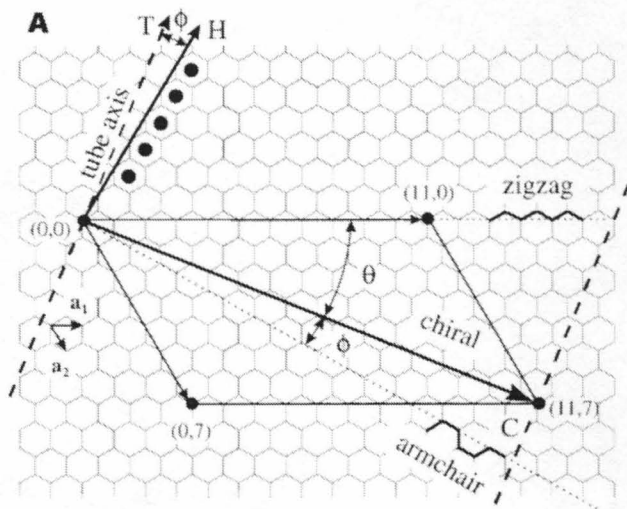


Fig 2: The unrolled honey comb lattice which shows the chiral vector C_h [1].

The Chiral angle varies between 0^0 - 30^0 . In particular, if $m = 0$ (and $\theta = 0$), the SWNTs are zigzag tubes. If $n = m$, the SWNTs are armchair tubes. All other SWNTs are chiral tubes. Following figure shows the classification.

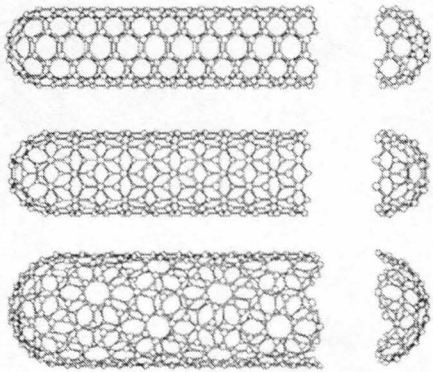


Fig 3: A (5, 5) armchair nanotube (Top), a (9, 0) zigzag nanotube (middle) and a (10, 5) chiral nanotube. The diameter of the nanotubes depends on the values of n and m [2].

Integers n and m denote the indices of the primitive translation vectors in the honey-comb crystal lattice of graphene. The Chiral angle θ , is given by the scalar product of the chiral vector and the primitive translational vector:

$$\cos \theta = \mathbf{C}_h \cdot \mathbf{a}_1 / |\mathbf{C}_h| \cdot |\mathbf{a}_1| = (2n + m) / 2 \sqrt{(n^2 + m^2 + nm)}$$

The diameter of a SWNT is given by $d = |\mathbf{C}_h| / \pi = a / \pi \sqrt{(n^2 + m^2 + nm)}$ where a is $\sqrt{3}$ times the C-C bond length ($\sim 1.2 \text{ \AA}$).

Further more, the circumference of a nanotube is given by $|\mathbf{C}_h| = a \sqrt{(n^2 + m^2 + nm)}$.

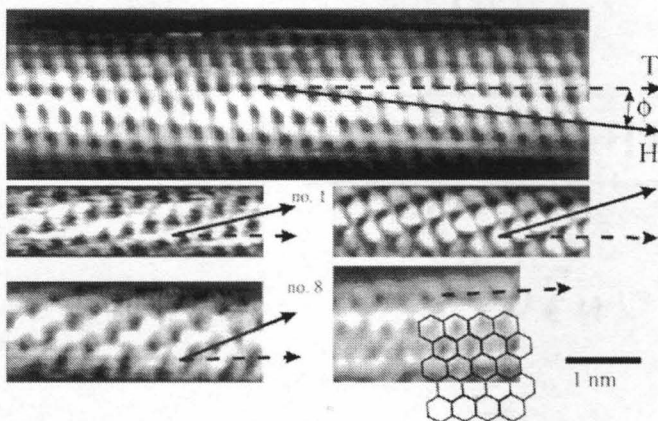


Fig 4: Atomsically resolved STM images of individual SWNT have shown in the diagram below [1].

The solid arrows indicate the direction of the nearest-neighbor hexagon rows \mathbf{H} and the dashed arrows indicate the tube axis \mathbf{T} . The top three tubes are chiral whereas the bottom two (from left to right) are zigzag and armchair respectively. The top figure has a chiral

angle of 7° and a tube diameter of 1.3nm which is a (11,7) type chiral tube. The hexagonal lattice is drawn in bottom right figure to ensure a non-chiral armchair structure[1]. As shown in the above figure, Scanning tunneling microscopy (STM) and spectroscopy images of single-walled nanotubes have helped to reveal electronic properties as a function of tube diameter and wrapping angle. Surprisingly, slight alterations of these parameters lead to a shift from metallic behavior to a semiconducting behavior. Theoretical calculations predict that armchair ($n=m$) tubes have conduction and valence bands crossing the Fermi-level which gives metallic tubes while other tubes have less number of bands near the Fermi-level which corresponds to semiconducting tubes. The following two graphs show the conduction/valence band variation along the change in Density of States (DOS) with the energy. More theoretical aspects will be considered of density of states in the next section.

Metallic Tube

Semiconducting Tube

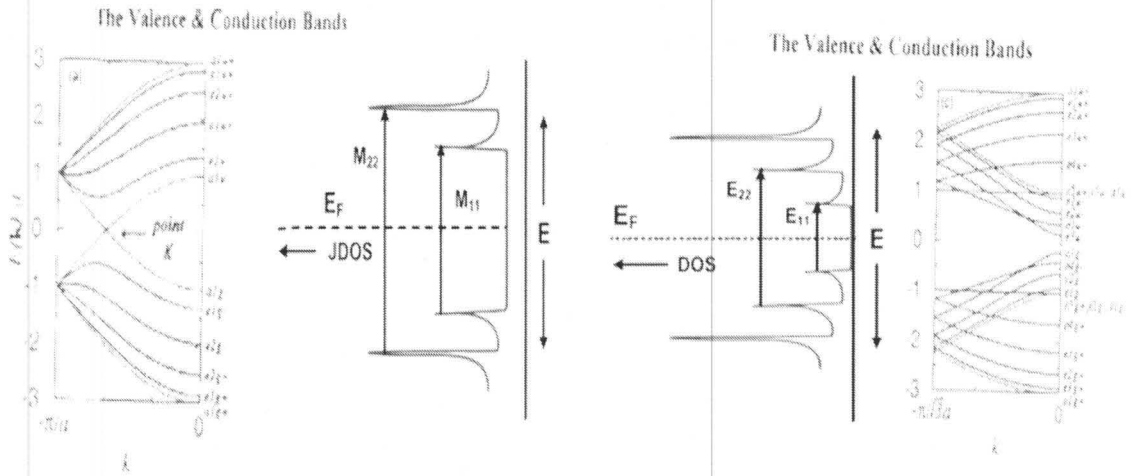


Fig 5: The figure shows the less number of states near the metallic tubes and large number of states near the semiconducting tubes which agree with the theoretical predictions.

Tubes other than armchair (chiral and zigzag) have two possibilities. When $n-m = 3l$ (l is any integer), tubes are metallic and If $n-m \neq 3l$, tubes are said to be semiconducting. The energy dispersion calculation results show that about one third of tubes are metallic and the rest of the tubes show a semiconducting behavior. The metallic to semiconducting ratio of the tubes also depends on synthesis methods and techniques which will be dealt in later of this report. The energy gap of the semiconducting single-walled carbon nanotubes is of the order of 0.5-0.6 eV which only depends on its tube diameter. This is given by the relation;

$$E_g = 2\gamma_0 a_{c-c}/d \quad \text{where} \quad \gamma_0 \text{ is the C-C tight binding overlap energy, } a_{c-c} \text{ the nearest-neighbour C-C distance } (\sim 1.42 \text{ \AA}) \text{ and } d \text{ is the diameter of the tube.}$$

According to the above relation, when the diameter of the nanotube increases, more wave vectors allowed (i.e. more number of states) within the gap which leads to a decrease in energy gap.

Band Structure and Density of States of Single-walled carbon nanotubes

As far as the electronic structure is concerned, carbon nanotubes can be either semiconducting or metallic depending on its diameter and chirality as discussed in previous section [3]. Also the gap of the semiconducting nanotubes is inversely proportional to its diameter which can be analyzed by electrical characterization of nanotubes. The energy dispersion relations of CNTs can be studied by 2-D graphite layer which is an approximation of 3-D hexagonal graphite structure. The following diagram shows the unit cell (a) and the first Brillouin zone (b) of graphite. The energy dispersion relations are obtained along the perimeter of the Brillouin zone as shown in figure 1.6 (b) where Γ KM are symmetry points within the first Brillouin zone.

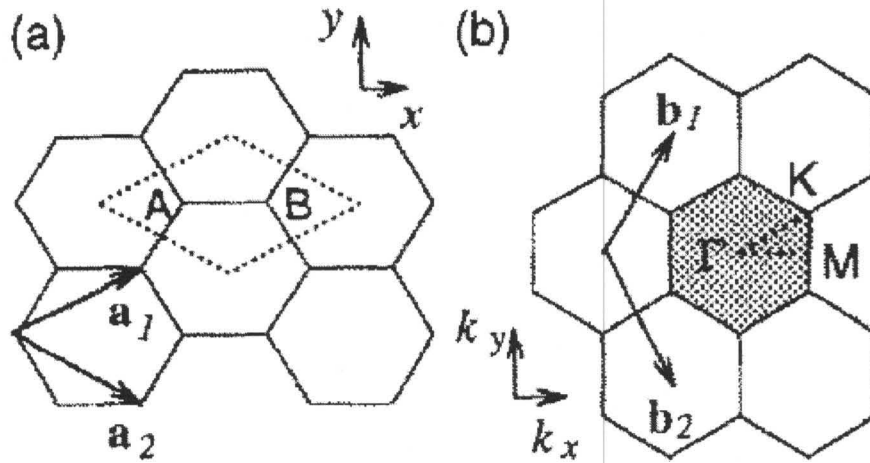


Fig 6: (a).The unit cell of the 2-D graphene is shown in the dotted rhombus and the \mathbf{a}_1 , \mathbf{a}_2 represent the primitive lattice vectors. (b). This figure shows the reciprocal lattice of 2-D graphene and shaded pentagon represents the first Brillouin zone.

The energy dispersion relation for a 2-D graphene sheet can be written as the

$$E = \pm \gamma_0 \left(1 \pm 4 \cos\left(\frac{q\pi}{n}\right) \cos\left(\frac{ka}{2}\right) + 4 \cos^2\left(\frac{ka}{2}\right) \right)^{1/2} \quad \text{for armchair tubes}$$

Where $-\pi < ka < \pi$, $q = 1, 2, \dots, 2n$.

$$E = \pm \gamma_0 \left(1 \pm 4 \cos\left(\frac{q\pi}{n}\right) \cos\left(\frac{\sqrt{3}ka}{2}\right) + 4 \cos^2\left(\frac{q\pi}{2}\right) \right)^{1/2} \text{ for zig-zag tubes}$$

Where $-\pi/\sqrt{3} < ka < \pi/\sqrt{3}$, $q = 1, 2, \dots, 2n$.

$$E = \pm \gamma_0 \left(1 \pm 4 \cos\left(\frac{q\pi}{n} - \frac{mka}{2n}\right) \cos\left(\frac{ka}{2}\right) + 4 \cos^2\left(\frac{ka}{2}\right) \right)^{1/2} \text{ for chiral}$$

tubes where $\pi < ka < 2\pi$.

The calculations are done using the tight-binding model. Even though, this model is not described here, the result of the dispersion relation is shown in the following diagram.

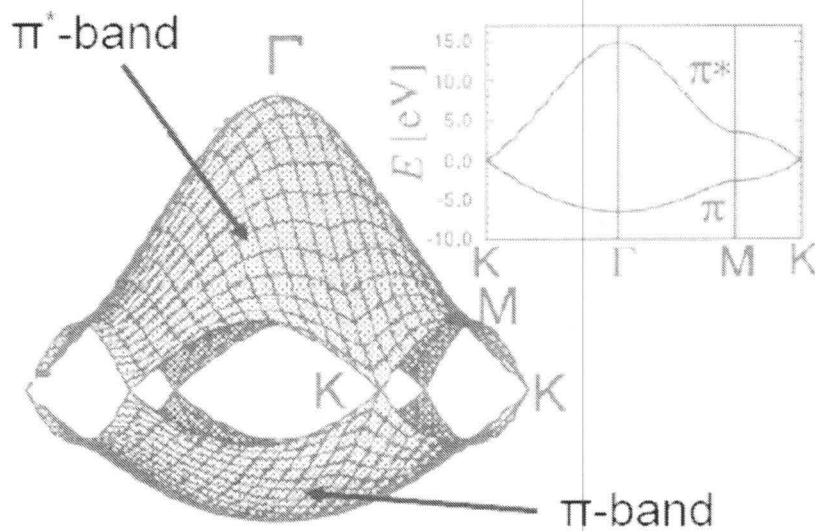


Fig 7: Energy band relation of 2-D graphene sheet for the first Brillouin zone. The inset shows variation of energy along the symmetry edges of Γ KM.

The lower half of the dispersion curve corresponds to π -bonding band and the upper half corresponds to π^* anti-bonding band. Graphene has 2 atoms per unit cell so only these π electrons are responsible for electrical conduction (valence electrons). Conduction band/Valence band touch at six edges of the hexagon which corresponds to K points as shown above. According to the above dispersion relations, the energy dispersion relations can be plotted for any indices of armchair, zigzag and chiral nanotubes.

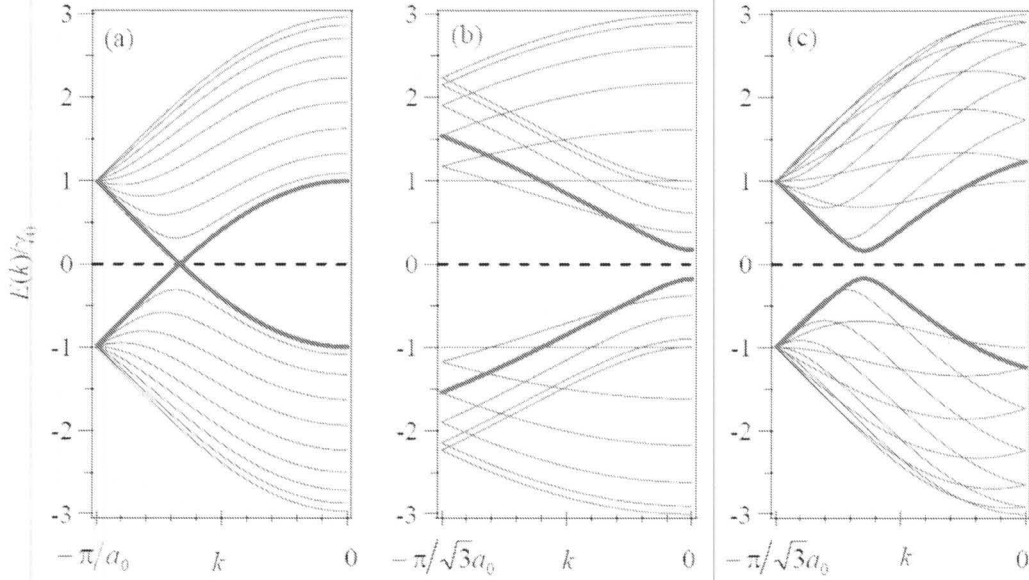


Fig 8: Energy dispersion curves for armchair(10,10), zigzag(10,0) and chiral(6,4) nanotubes[4]

For metallic nanotubes the relation for the Density of States per unit length along the tube axis is given by

$N(E_F) = (8/\sqrt{3})a\gamma_0$ where a is the lattice constant and γ_0 , the nearest C-C tight binding overlap energy ($\sim 2.5\text{eV}$ for 2-D case) [3].

1-D density of states for 2-D graphene sheet is shown in the diagram below. The metallic tubes have small non-zero DOS at Fermi level which is at energy $E=0$ but semiconducting tubes have zero DOS at Fermi level as shown below.

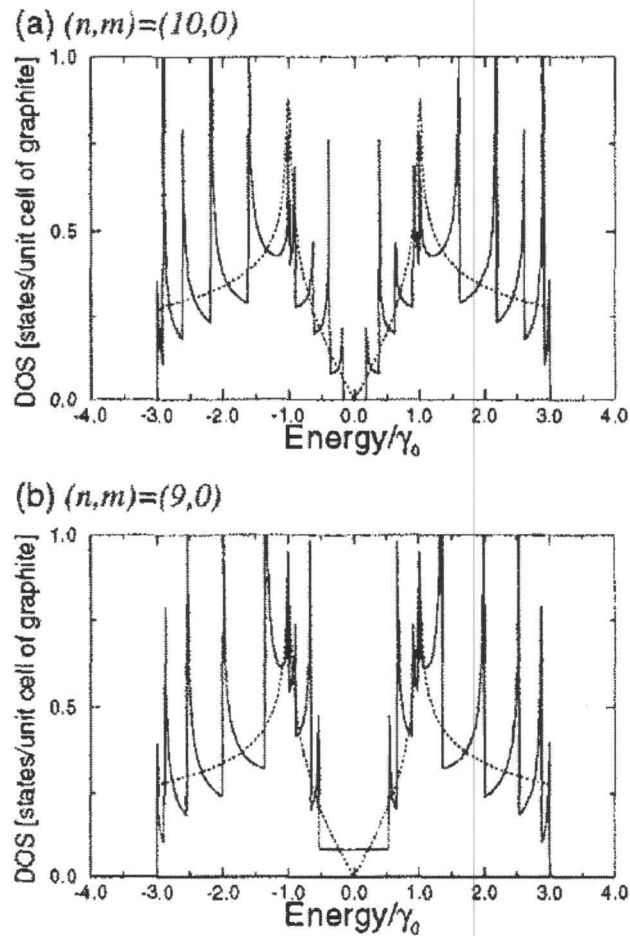


Fig 9: 1-D DOS for 2-D graphene sheet is shown for (a) (9,0) metallic and (b) (10,0) semiconducting nanotubes. The dotted lines are the DOS for 2-D graphene layer[3].

Synthesis of Carbon Nanotubes

Techniques involving synthesizing of carbon nanotubes depend on the current applications in different fields. Field-emission based applications such as in LCD display units require the growth of carbon nanotubes in highly aligned bunches, in highly ordered arrays or located at specific locations. For this, growth of nanotubes does not need mass

production but controlled growth and purity with a specific texture. Hence structural quality of SWNTs, the purity of nanotubes and the control of configuration (chirality) are one of the main conditions adapted to applications. On the other hand these are infact the problems involving in synthesis of nanotubes using different techniques.

By considering large number of experimental parameters and conditions, techniques of nanotube growth can be divided into two classes namely, Solid carbon-source based production techniques and Gaseous carbon-source production techniques of nanotubes.

1. Solid carbon-source based techniques
 - a. Laser ablation techniques.
 - b. Solar energy furnace.
 - c. Arc discharge techniques.

The common points for above mentioned techniques are that the temperature ranges from 1000K to 6000K and the carbon source originates from solid graphite. Other than these two parameters, the structure and the SWNTs yield can be altered up to certain limit by the other experimental conditions.

Laser ablation technique

Both Pulse mode and continuous mode laser devices are used to utilize the carbon nanotube growth by modifying the methodology by large number of researches. Principle technique involves graphite pellet containing catalyst placed in middle of gas-filled quartz chamber in a furnace temperature of 1200⁰C. By focusing the laser beam on to this

pellet allows the catalyst to vaporize and bombard the graphite surface. The flow of neutral gas makes the carbon species deposited in several regions inside the chamber as dirt. Several modifications have been added to this principle setup to improve the efficiency of the nanotube growth. For an example, an additional pulse laser beam is introduced to the chamber which allows bombarding the pellet. The purpose of this second beam is to vaporize the aggregates produced by the first ablation. Reactor with a continuous CO₂ laser device is shown in the next page.

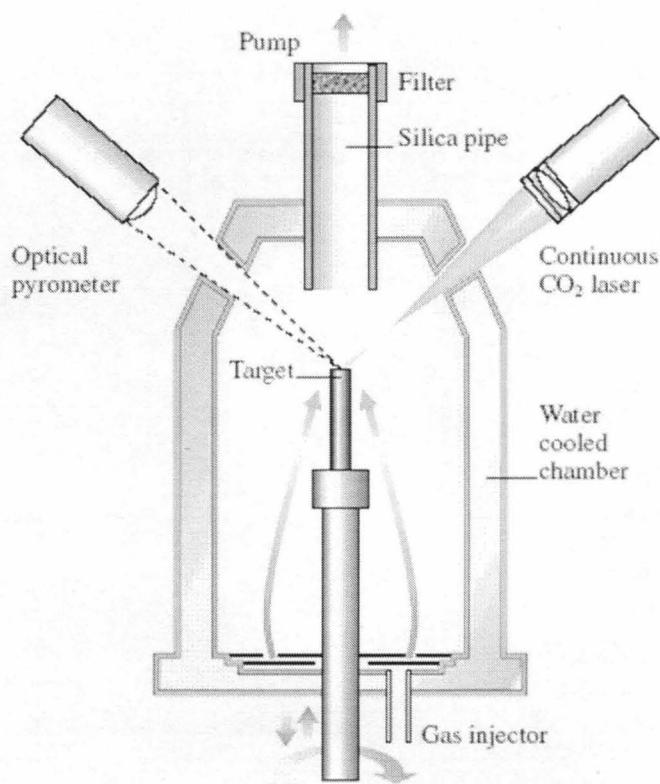


Fig 10: Reactor used to produce SWNT using Laser ablation method.

The quantity of SWNT depends on the type of metal catalysts used. When using the small quantities of Ni and Co (transition metals), the SWNT growth will occur and this yield increase with the furnace temperature. The quantity and quality increase dramatically

with the furnace temperature and the best quality SWNTs is produced at the furnace temperature at 1200 °C. at low temperatures the SWNTs show poor quality and defects occurred due to amorphous carbon which is one of the main issues comes with the SWNT structures. MWNTs can be obtained using this method with the absence of catalysts which have length up to about 300nm. One of the main advantages of this technique involved nanotubes is that it gives high quality SWNTs with 5-20nm in diameter and from 10 to 100 of micrometers in length. Because of the cleanness/quality and high aspect ratio of nanotube production, the laser ablation (vaporization) technique has been considered as one of the major methods in commercial world to produce SWNTs.

Solar furnace

The principle technique of this method is that the solar rays are collected by plain mirror and then it is reflected to a graphite pellet which is placed in a chamber called crucible. Due to the temperature of about 4000 K, under controlled atmospheric pressure, the catalyst and the carbon are vaporized and carried by the inert gas mixture deposited inside the walls of the reactor chamber. The graphite target (cylindrical tube) is designed to minimize the radiation losses which is called as thermal screen and act as a filter to amorphous carbon avoid depositing on the walls of the chamber. This graphite crucible is filled with graphite powder and catalysts. The carbon nanotubes obtained from this method are mostly MWNTs with bamboo texture, carbon shells and bundles of SWNTs using Ni/Co catalysts at low pressure. With Ni/Y catalysts and at high pressure, long SWNT bundles are obtained.

Arc Discharge Method

Arc discharge method is one of the major methods of commercially synthesizing SWNTs due to high quality and yield. But the yield and the quality of the SWNTs still depend on the experimental conditions and the type of catalysts used during the growth and most importantly on byproducts such as carbon nanoparticles, amorphous carbon nanofibers, multiwall shells and fullerene-like structures (C_{60}) and of course the catalysts remnants.

The Electric Arc reactor consists of a cylindrical reactor chamber with dimensions of about 30cm of diameter and 1m of height. Reactor has two terminals, one for the inert gas input and other for the vacuum pump. The pressure is maintained at around 0.1Pa. The side of chamber has a window to observe the arc created by two electrodes. Schematic diagram of the Electric arc reactor is shown below.

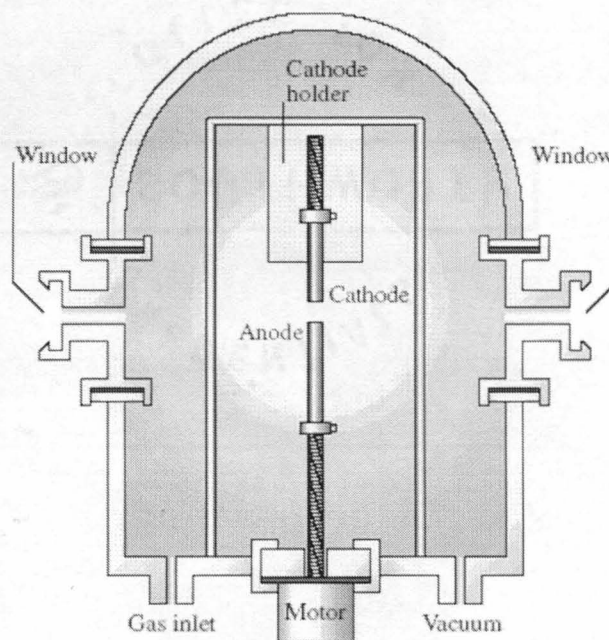


Fig 11: The diagram of an Electric Arc Reactor.

The electrodes designed in the chamber can be either vertical or horizontal. But vertical setup gives an advantage of being symmetry by the gravity. Both electrodes (anode and cathode) made up of graphite which the dimensions are in few millimeters and the potential difference is applied between the electrodes so that an electric arc is created. The anode can be either consists of mixture of graphite powder and catalysts or a coaxial hole consists of mixture of graphite powder and catalysts. Due to arc discharge, plasma is being created inside the chamber in the mixture of inert gas (He or Ar), carbon and catalysts vapour. The carbon nanotubes formed due to this plasmagenic gas are deposited inside the walls of the reactor and the anode is eroded at a rate depending on the power of the arc produced. But it does not necessarily give a higher yield with a higher erosion rate of the anode. Anyway the quality and yield of the formed nanotubes are depending on the arc current density, plasmagenic gas and of course the concentrations of the catalysts. [5]

2. Gaseous-carbon source based techniques

Gaseous-carbon source referred to the thermal cracking of carbon sources (hydrocarbon, CO) to produce nanotubes. The basic method involving this is CVD which stands for Chemical Vapour Deposition. CVD is the formation of thin solid films on a substrate material by chemical reaction of vapour phase precursor. CVD differs from other vapour deposition techniques such as Physical Vapour Deposition (PVD-Sputtering or Evaporation) in which atomic or molecular species of the substrate are involved in the nanotube formation. Chemical reaction in the vapour phase can be initiated by heat source such as inductive heater or furnace or even IR lamp (Thermal CVD), high

frequency radiation such as UV (Photo assisted CVD), or by plasma (Plasma-enhanced CVD). [6]

Chemical Vapour Deposition

Chemical vapour deposition described in this section referred to thermally initiated vapour phase chemical deposition which differs from plasma-enhanced CVD discussed later. CVD apparatus consists of a quartz tube with a diameter of about 1 to 2 inches which inserted into a tube furnace with a ramp rate of $\pm 1^{\circ}\text{C}$ over 25cm. Most CVD systems work in the atmospheric pressure so expensive vacuum pumps do not need in this case. A typical CVD reactor setup is shown in the diagram below.

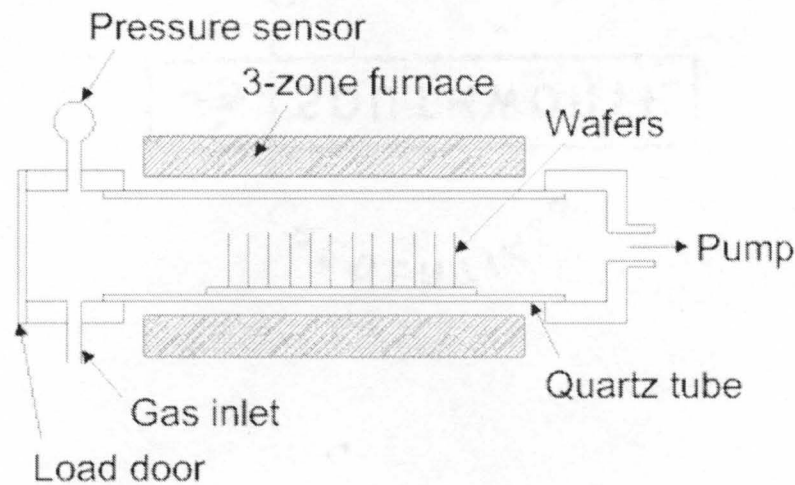


Fig 12: Schematic diagram of a CVD reactor.

Substrate of the dimensions of about 1 inch is placed inside the quartz tube and CO or hydrocarbons such as methane, ethane, ethylene, acetylene etc. are flown through a mass flow controller. In a typical growth, H_2 with an inert gas such as He or Ar or a mixture of

these gases are sent through the reactor until it reaches the desired temperature to grow the nanotubes and then the flow is switched to feedstock by mass flow controller for growth according to the specified recipe. Finally the flow is switched back to the inert gas until the chamber temperature reached to 300°C or below before exposing the substrate to ambient air. Exposure to air at temperature above room temperature might damage the grown nanotubes. Typical parameters of growth of nanotubes are vary from few nm/min to 2-5µm/min and the growth temperatures vary from 600°C to 1000°C which depend on the recipe [7]. This lower boundary of the temperature is critical to activate the catalyst for the growth of CNT.

Plasma-Enhanced CVD

Unlike thermal CVD, using PECVD the carbon nanotubes can be grown in low temperature. Recent articles show the growth of MWNT/MWNTF at temperature as low as 120°C. This is achieved, by 20% of methane with H₂ is introduced into the reactor that will contain higher hydrocarbons such as acetylene, ethane, and ethylene which need low activation temperature for the catalysts to grow CNTs. In contrast, thermal CVD working at 900°C will have only methane. As results of PECVD, free-standing, individual and vertically-oriented nanotubes can be achieved which is somewhat hard to obtain using thermal CVD. For this method several sources are used such as DC, Radio-frequency (RF), hot-filament aided with DC, and microwaves. In addition to the plasma source, mass flow controller and vacuum pumps are used in the setup. Water vapour is removed from the system by achieving a pressure of 10⁻⁸ Torr and base pressure below 100mTorr by turbo molecular pump. First the substrate is inserted in to the chamber and desired

temperature and pressure is obtained in the chamber for the growth. Then, the power source is coupled to plasma source while the inert gas is flowing through the chamber. Finally everything is turned-off except the gas flow until temperature decreases below desired values so that the substrate can be removed from the chamber. [7]

Purification

Synthesized carbon nanotubes which discussed in previous section may contain impurity materials specially amorphous carbon which is undesired by researchers. So Purification of nanotubes has been an important part in removing these unwanted materials from nanotubes so that they can be used in experiments. Heating, centrifugation and filtering are some of the earlier methods used which the purification was achieved up to some extent even though heating can cause an increase in tube diameter. Presently, Three main methods of Purification are known such as gas phase, liquid phase and intercalation methods.

The gas phase purification technique involves the removal of amorphous carbon by oxygen burning or oxidation process. MWNTs are purified using this method by slowly removing nanotube cylindrical structures layer-by-layer. Oxygen is more stable to graphene layers than does the amorphous materials, so that unwanted materials can be separated from nanotubes. Disadvantage of this method is that the small diameter tubes may oxidized with unwanted nano materials. Liquid phase method is the separation of nanotubes using Potassium Permanganate (KMnO_4) which has a higher yield than gas phase. Intercalation method is chemically removing the nanotubes by $\text{CuCl}_2\text{-KCl}$. This molecular solution is intercalated with open structures such as nanoparticles and

amorphous carbon and then it is chemically removed so that closed structures like nanotubes will be remained [3].

Characterization Techniques

Characterization techniques have been developed with revolutionary industrial and scientific applications of nanotechnology in the material science field. Modern techniques in characterizing materials give the researchers more information up to the nanoscale of the material being analyzed which not only makes a better understanding of the underlying mechanism, but also gives a better insight of new applications [8]. Characterization techniques can be either electrical or optical depending on the technique and the property of the material being characterized. Only few, among many characterization techniques will be discussed in this section which used in experimental chapter.

In electrical characterization, I-V measurements within ohmic contacts play a major role. Other than that, C-V (Capacitance-Voltage) junction measurements, deep level transient spectroscopy (DLTS) and Photo-induced current transient spectroscopy (PICTS) measurements revealed information of barrier heights, majority carrier deep traps such as energy and majority and minority carrier deep traps respectively. I-V measurements reveal the resistivity and current transport models of the materials. Investigating electronic structures of materials, Scanning Electron Microscopy (SEM), Tunneling Electron Microscopy (TEM), Raman Spectroscopy, Atomic Force Microscopy (AFM) and X-ray diffraction techniques are main methodologies used at present. Other than that

optical microscopy (OM) and Photoluminescence measurements such as μ -PL are also used in electrical and optical characterization of materials.

Transmission Electron Microscopy (TEM)

There are several reasons of which the electrons being used for understanding the material structures. Higher resolutions allowing due to the small wavelengths of electrons (\sim up to few picoameters), production of much information by secondary waves coming from the materials as a result of interactions with matters are major reasons the transmission electron microscopy being popular among researchers. Lattice structures, lattice parameters, defect distributions and chemical information of atomic regions are revealed using TEM measurements. Electron microscope consists of an electron source and several magnetic lenses as in figure below.

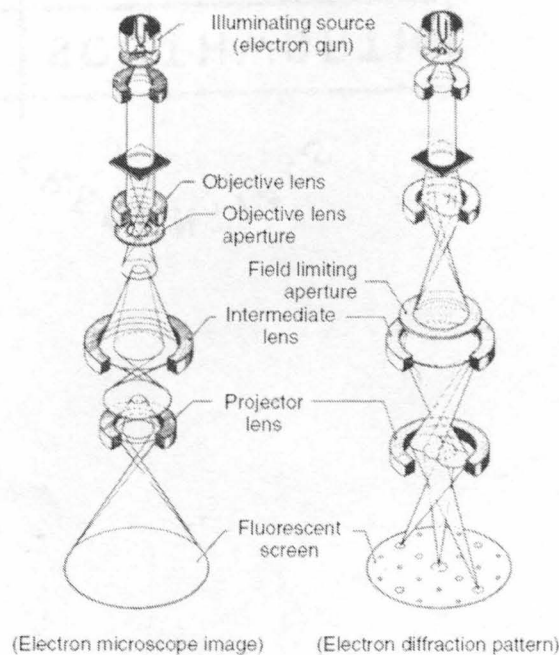


Fig 13: The electron ray and the diffraction pattern diagram of a TEM.

There are two sources of which the electrons are produced. Thermo ionic (TI), that emit electrons when heated (which can be a tungsten filament) and Field emission (FE), that emits electrons when an electric field is applied (which can be a fine needle). There are characteristic differences between these two when act as electron sources in TEM. TI gives less monochromatic wavelength than FE but they are inexpensive. FE sources are coherent and give a higher current density. The diffraction pattern formed by a particular region of a specimen is chosen by an aperture which is next to the objective lens. This chosen area is called Selected Area Diffraction (SAD). If transmitted beam from the objective lens pass through this aperture, resulting SAD pattern will contain a series of bright spots, (which refers to bright field (BF)). If one diffracted beam is passing through the aperture, the SAD will contain dark field (DF). The objective lens is converging lens of which the aperture is located at the back focal plane of the objective lens. Finally this diffraction pattern is magnified and sends to a display unit. The charged electrons coming from the electron gun by help of high voltage (100-1500KV) will interact with object atoms and diffracted according to Bragg's law. This diffracted beam (secondary signals) gives information such as lattice parameters and structures of the materials being analyzed. The electron lens is used to increase the depth of field of instrument. That is the images can be obtained from top to bottom of the material which is an advantage of TEM. One of the major disadvantages of this method are higher the resolution of the TEM image, smaller the portion of the material one can analyzed which does not give a good understanding of the material. Also to get a TEM image, the sample must be thin enough so that electrons can pass through to create a pattern which is practically difficult

to achieve. For an example, to get a TEM image, a GaAs sample must be less than 50nm that transparency of that gives in just 0.5microns [8].

Scanning Electron Microscopy

Scanning electron microscope is one of the most widely used instruments in material characterization due to several reasons. User-friendly equipment setup, higher resolution images (up to 0.5nm) and large compatibility of specimen sizes that allowed microscopy are some of the advantages of this equipment. Other important property of SEM is that by passing a single beam of electron, we can collect multiple secondary beams from several portions of images of the same sample by multiple detectors and display as a combined image or an individual image at the same time which is very useful and accurate in characterization of materials. The basic schematic diagram diagram of a SEM is shown in the following page.

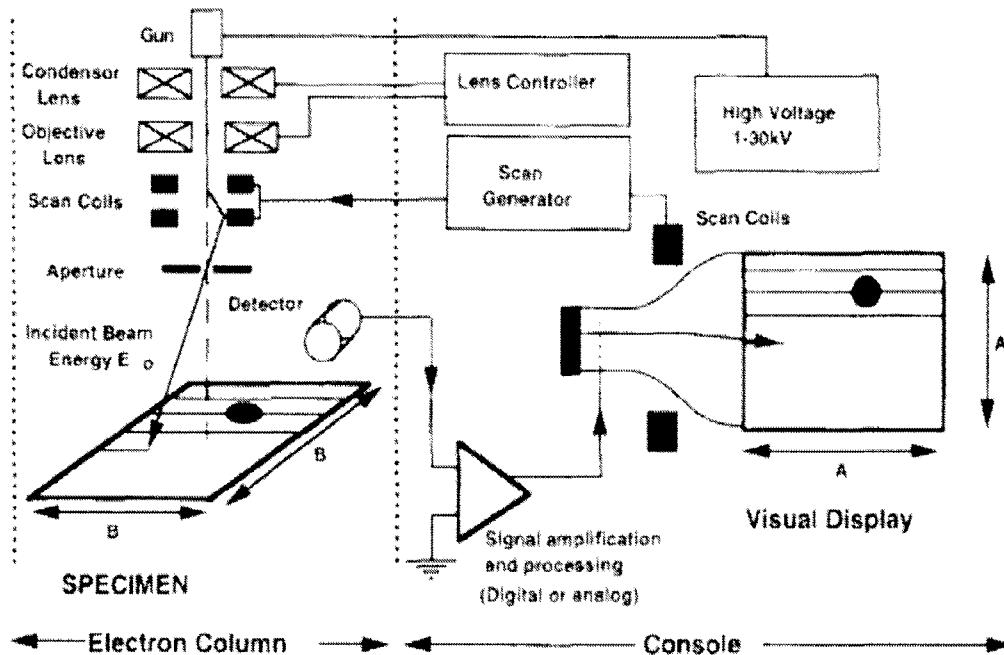


Fig 14: A schematic diagram of basic components of a SEM.

A SEM machine can be basically divided into two components namely, electro-optical detector system and scanning, processing and display systems which refer to electron column and console column respectively. An electron beam produced by an electron gun either by thermo ionic or field-emission described under TEM, is accelerated by high voltage in the range 500eV-30keV are passed through electromagnetic lenses (or electrostatic lenses. Modern SEMs use electro-magnetic lens) allowed to strike the specimen being analyzed. Unlike TEM, the electron beam of the SEM is scanned across the sample and the secondary beam which is coming from the sample is being magnified along with the incident beam. As shown in the diagram, the scan coils in the electron-column scan the specimen line-by-line. Then a detector used to send those to an amplification circuit which magnifies the signals and send to a display unit. The scanned pattern is usually consists of 1000 horizontal lines each has 1000 points or pixels. So the final image will be magnified in the range of 10^6 . ADC (analog-to-digital converter) is present in the console column so that images can be enhanced and stored digitally in a computer.

Raman Spectroscopy

It is worthwhile to understand the basic mechanism of Raman spectroscopy prior to the use of the technique. Raman Scattering is due to the inelastic scattering of light from nanotubes or whatever material being analyzed. The energy of the scattered light will be increased or decreased due to the emission or absorption of phonons (lattice vibrations) in nanotubes[7]. Generally, the scattered light is less than the incident light because of the

phonon energy and this scattered light intensity is plotted as a function of frequency of the scattered light which is called Raman spectra. By observing Raman spectra, we can reveal information about phonon frequencies of the materials. Raman scattering can be either due to emission or absorption of phonon which are called Stokes or anti-Stokes processes respectively. Raman can be not only due to phonon, but also due to elementary excitations such as magnon or plasmon. Both discrete and continuous high power ($40 \times 10^9 \text{ W m}^{-2}$) laser are being used to probe the SWNTs which are stable in high temperatures. Ar-Kr and He-Ne lasers are used as to get discrete lines and Ti, Sapphire and Dye are used as to get continuous lines in the Raman spectra. But the power of laser beam is depend on the stability of the material to heat which is obvious in this case. The number of phonons scattered in inelastic scattering is known as the order of Raman processes. If one phonon is scattered because of light, then it is a first order Raman process and if two phonons are scattered then it is a second order Raman process and so forth. In SWNTs the Raman spectra have some prominent features. At around 1580 cm^{-1} the spectrum shows a narrow peak which is called as G-band. Another low frequency peak occurs in Raman spectrum at around 150 cm^{-1} (100 cm^{-1} - 500 cm^{-1}) which is called Radial Breathing Mode (RBM), ω_{RBM} . Both these features are due to first order Raman processes for SWNTs. The following Raman spectra is a result of SWNT bundle sample.

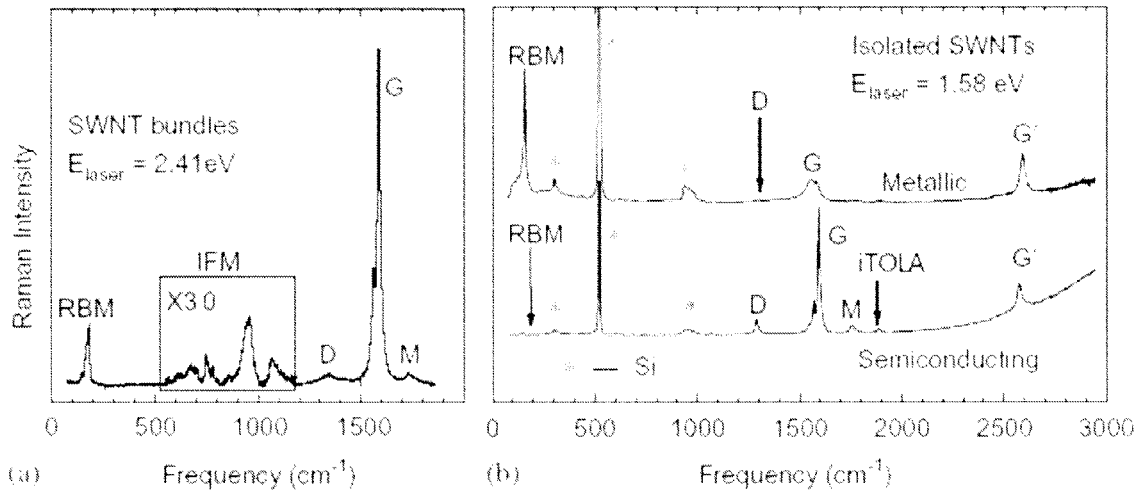


Fig 15: Raman spectra of (a) HiPco SWNT bundle and (b) metallic and semiconducting isolated SWNTs.

Addition to G-band and RBM, there are several other weak features in a Raman Spectrum. A combination of optical and acoustic modes is occurred at around 1900cm-1 as shown in the spectrum is called iTOLA band which is a second order mode. The D and G' bands are also belong to RBM. The Radial Breathing Mode occurs due to coherent vibrations of C atoms in the radial direction. The name comes from the shape the vibration occurs (like breathing). RBM frequency used to study whether material consists of SWNTs and to study the diameter and electronic structure. The RBM frequency is given by ω_{RBM} , where $\omega_{RBM} = A/d_t + B$. (A and B constants are determined experimentally). Most importantly ω_{RBM} used to characterize the ratio of metallic to semiconducting of a SWNT sample which is useful in material characterization[9].

Atomic Force Microscopy

AFM has been very useful in imaging isolated SWNT prepared on a silicon substrate or SWNT bundles prepared by CVD. Even though AFM does not give high resolution like TEM, so many details can be derived which is useful in structures and device preparation using CNTs. Also the tips used in AFM machines are replaced now by SWNT which has unique properties compared to conventional tips been used in AFM. 1-D nature and ability of SWNTs to be stable in mechanical pressure due to impact with sample allow improving the technique very much [7].

In AFM atomic resolution of the material being analyzed by a tip that is close to the surface of the material. This tip is connected to a microfabricated cantilever of which the deflection is being measured. In non-contact AFM method, a tip-sample force created due to the potential energy and distance is used to image the signal. The cantilever deflection due to this force is measured by optical (interferometer, beam bounce) or electrical methods (piezoresistive, piezoelectric method). NC-AFM or Tapping mode-AFM is popular among researchers because of true resolution images, ability to measure insulating surfaces and mechanical properties like elastic deformation. AFM operating mode can be classified as static or dynamic depending on how the signal is interpreted by the cantilever. In static mode, the force converted into deflection of the cantilever which depends on the spring constant of cantilever. This small value of spring constant (k) increases the force sensitivity and the deflection of the cantilever should be larger compared to the deformation of tip or sample. For this to occur, the cantilever should be soft unlike the bonds between the atoms in tip as well as the in the sample. The dynamic mode can be either amplitude modulated (AM) or frequency modulated (FM). In AM

mode, the actuator is vibrated at fixed amplitude with a fixed frequency. The elastic and inelastic interactions occur due to the proximity of the tip would change the amplitude and phase of the cantilever which is amplified as the signal for the image. But a delay would occur by this method depends on the noise. To overcome this issue, FM mode developed to increase the speed. Addition to the speed, FM mode gives a better resolution and less noise by reducing the proximity between the tip and the sample [5].

Applications of Nanotubes

Carbon nanotubes have invaded almost all fields in today technology and industry. Many applications have improved and developed due to their dramatic electrical, optical, mechanical and other properties. Carbon nanotubes are widely used as chemical sensors, physical sensors, bio-sensors, composite materials and in nanoelectronic applications.

Chemical/Physical/Bio Sensors

Carbon nanotubes can be used as very small gas sensitive devices to environmental conditions because of its dependence to electronic properties and structure. Not only the sensitivity, but also the accuracy and fast response of these devices make the sensor technology more developed than any other fields.

When the electronic structure of graphite is considered, it has a linear structure with π -electrons from sp^2 hybridization distributed symmetrically around C-C bonds. In contrast, π -electron cloud in CNTs are somewhat distorted therefore asymmetrically distributed around the C-C bond. Due to this polarization, the CNTs are electrochemically active. So

when the electron donors (molecules which are desired for electron donations) or acceptors (molecules which are desired for electron receiving) are close enough to these electron clouds, charge carriers (electrons or holes) may induced to transport from CNTs to environmental gas or vice versa. Further more, these gas molecules can be bonded to the nanotubes in surfaces of their structures or internally. Due to the strength of bond between the gas molecule and CNT, the nature of absorption can be divided into two categories, namely Physisorption in which the molecules are bonded by weak Van der Waals bonds or Chemisorption, a strong/intermediate adhesion by chemical bond such as ionic due to charge transfer [10]. This will result of change in electrical parameters such as conductance (or resistance), thermoelectric power (TEP) and etc which can be measured by electrical characterization techniques. Molecules such as oxygen and ammonia are more sensitive to CNTs under this mechanism which is used by many research groups in studying gas sensors. The Field Effect Transistors (FETs) made using single SWNT is used in many fields as an application. The following diagram shows a microfabricated SWNT FET using a Silicon substrate. I_{ds} - V_{ds} characteristics are measured using the poly-silicon as gate in between Gold (Au) drain source pads.

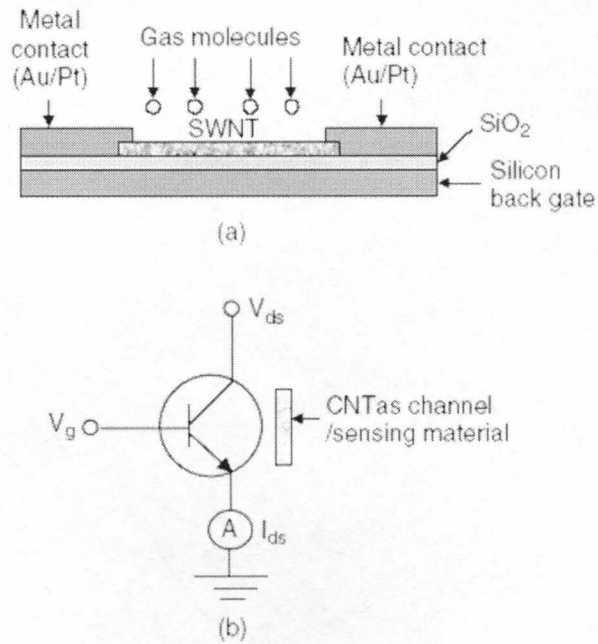
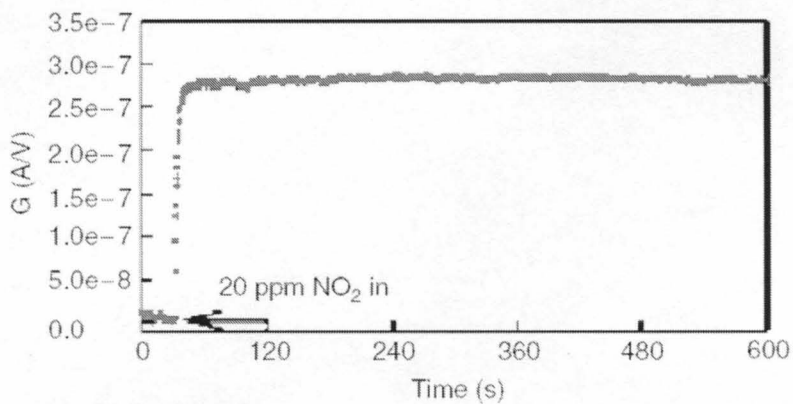
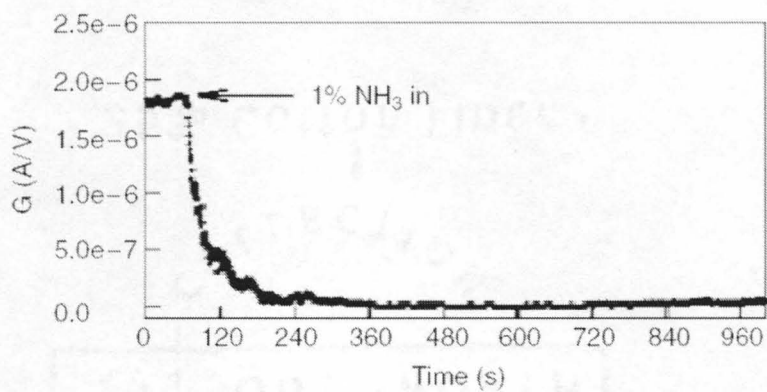


Fig 16: Schematic diagram of a microfabricated FET using a single SWNT [7].

The sensitivity of these FETs is measured in the exposure to oxygen, ammonia and Hydrazine by measuring I-V characteristics. The following graphs show the change in conductance due to exposure of NO_2 and NH_3 for SWNT FET sensor.



(a)



(b)

Fig 17: The change in Conductance due to exposure of NO_2 (20 ppm) and NH_3 (1 %) gases.

CNTs can be used as bio-sensing devices because of its small size. CNTs are used as probes that inserted into cells without disturbing its metabolism to obtain details of mechanisms and disease infections with high sensitivity. FET based bio-sensors are used to obtain details due to high sensitivity to binding with charge species in molecules.

Thermoelectric power of Metals and Semiconductors

Thermoelectric power is the measurement of potential difference due to a temperature gradient across a sample. The thermoelectric power S is given by

$$S = \frac{\Delta V}{\Delta T}$$

Where ΔV , the potential difference across the sample and ΔT is the temperature gradient.

When a heat pulse is given to a conducting material, electrons at the hot end gain high energy than that at cold end. Due to this effect an extra electrons are accumulated at the cold end by diffusing from hot end which is called diffusion current. As a result a potential difference or electric field can occur between two ends. This electric field builds up until equilibrium occurs between the diffusion and electrostatic field.

Using the Fermi-Dirac statistics and Boltzmann transport equation a metal conductor thermoelectric power can be written as

$$S = \frac{1}{eT} \frac{\int dk \tau(k) v(k) v(k) [\varepsilon(k) - E_F] \left(\frac{\partial f}{\partial \varepsilon}\right)_{\varepsilon=\varepsilon(k)}}{\int dk \tau(k) v(k) v(k) \left(\frac{\partial f}{\partial \varepsilon}\right)_{\varepsilon=\varepsilon(k)}}$$

where T electron relaxation time and v is the electron group velocity, f is the equilibrium distribution function, e is the electronic charge and ε is the electron energy with respect to the E_f . Above expression leads to the following expression which shows a linear temperature dependence to thermoelectricity.

$$S = - \frac{\pi^2 k_B^2 T}{3e} \left(\frac{d \ln \sigma(E)}{dE} \right)_{E=E_F}$$

$\sigma(E)$ is the electrical conductivity as a function of electron energy E. this is so called the Mott relation for thermoelectric power.

Where $\sigma(E) = e^2 v(E)^2 N(E) \tau(E)$. Here the N(E) is the density of states. The Mott relation can be modified as

$$S = - \frac{\pi^2 k_B^2 T}{3e E_F} \left(\frac{3}{2} + m \right)$$

where m is the number that depends on the type of scattering that is dominant. For

example in phonon scattering region (high T) $S = - \frac{\pi^2 k_B^2 T}{3e E_F}$

Thermoelectric power for semiconductors is different to that of metals. The thermoelectric power using Boltzmann statistics can be written as

$$S = \frac{k_B}{e} \left[\frac{E_c - E_F}{k_B T} + A_c \right] ; E > E_c$$

$$S = \frac{k_B}{e} \left[\frac{E_c - E_F}{k_B T} + A_c \right] ; E > E_c$$

where A_c and A_v are temperature independent constants. These are true for non-degenerate (few conduction electrons) semiconductors which can be written in general as

$$S = \frac{k_B}{e} \left[\frac{|\lambda|}{T} + \beta \right]$$

Where β is a constant (this constant equals to 3 when both density of states and mobility increases linearly with E and 1 when both DOS and mobility are constants.). Hence from this equation we can say that thermoelectric power is inversely proportional to T.

experimentally it is found that TEP of a semiconductor is large at room temperature (mV/K) and for metals it is small ($\mu\text{V}/\text{K}$) [4].

CHAPTER 2: EXPERIMENTAL TECHNIQUES

Intrinsic properties of single-walled carbon nanotubes have shown amazing properties compared to other nanostructures. In studying these intrinsic properties, electronic parameter measurements play a main role in understanding the properties. In this chapter we report experimental studies of charge transport properties of single-walled carbon nanotubes by thermoelectric power and four probe measurements.

Preparation of thin films of SWCNT

The single-walled carbon nanotubes were synthesized using Pulse laser vaporization technique which was discussed in the introductory chapter. In the sample preparation, first, small amount of SWNT powder was added to Dimethylformamide (DMF) in a beaker and sonicated for about 30 minutes. Then It was centrifuged for about 3 minutes at a speed of 10x1000rpm. Secondly, this solution of SWNT was deposited on a glass substrate (SiO_2) of the dimensions 10x5mm by drop casting method. The sample was lightly heated while depositing until a clear thin film of SWNT was visible on the glass substrate. The impedance across the sample was found to be 10K Ω . Next the sample was mounted on the sample holder by applying small amount of varnish. Varnish has a poor electrical conductivity and good thermal conductivity.

Two K-type thermocouples (Chromel/Alumel) were used to measure the Thermoelectric power in the experiment. K type was chosen due to its high sensitivity level ($40.6\mu\text{V}/^\circ\text{C}$ at 25°C) over a large temperature range (270°C to 1300°C). Two K-type thermocouples, two Copper(Cu) leads and a Platinum(Pt) heater were attached to the sample with small amount of Silver(Ag) epoxy at the four corners.

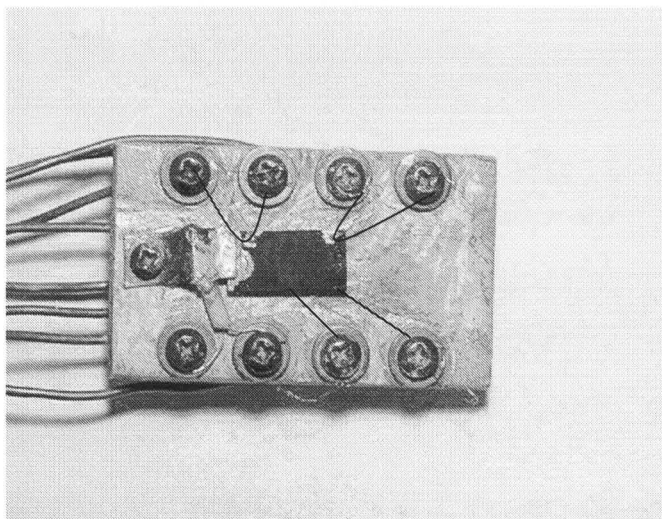


Fig 18: The Sample with the probe (The Pt heater is connected to one edge of the sample).

This sample holder was extended to a probe which contains a head with hermetic multi-pin connector for electrical input/output. The probe was contained in a quartz reactor which is connected to a turbo molecular pump. Also the reactor has provisions for controlled gas exposure/evacuation.

Basic Experimental Setup

The Basic experimental setup consisted of the Thermopower/Resistance Reactor, the Heat-pulse Generator, Turbo-molecular pump, Mechanical pump gas handling system and the Tube furnace.

The Thermopower reactor consists of about 25cm in length and 20mm inner diameter quartz chamber with a 2 ³/₄ in. knife-edge flange sealed via a Cu gasket to a standard multipin feed through flange[11].

The thermopower measurement system is shown in the following schematic figure. The heat pulse generator was used to generate a time-dependant temperature difference between the thermocouple junctions in the sample. The heater used was a simple Platinum(Pt) resistor of which one end was connected to the sample by a heater cover and the other end was connected to the heat pulse generator. This heat pulse generator is a PIC 16C56 micro controller which produced voltage pulses with different pulse heights and widths[12]. An improved Analogue subtraction circuit was used to obtain the measurements of thermoelectric power of which the schematic diagram is shown below.

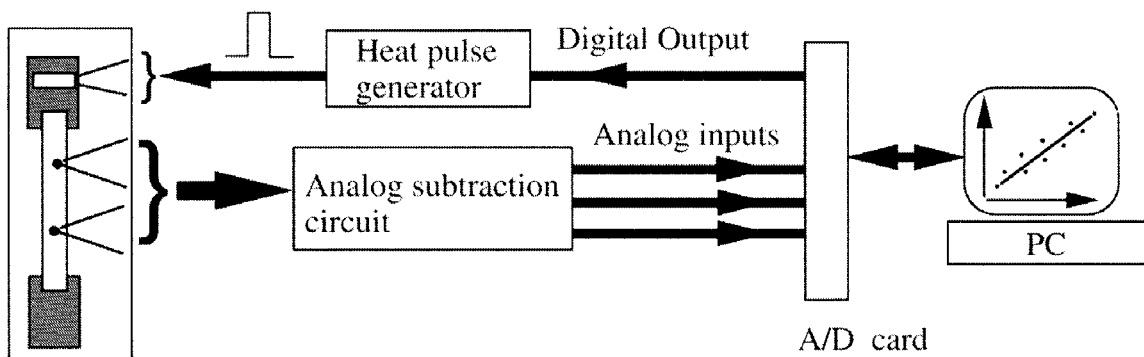


Fig 19: Figure of schematic diagram of the Analogue subtraction circuit.

In this analogue subtraction circuit, three Analogue Devices Inc. AD620 instrumentation amplifiers are used namely A1,A2 and A3 as shown in the diagram below. Amplifiers A1 and A3 used to have a gain(G) of 1000 while A4 has a gain(g) of 10. variable resistors R1 and R3 used to have their gains matched. The voltage difference ΔV_2 which is coming from the amplifier A2 with the gain g_T is used to measure the average temperature of the sample. The amplifier outputs Y_A , Y_B , X and Z (which is used to measure the sample temperature) are fed to the computer for processing[12].

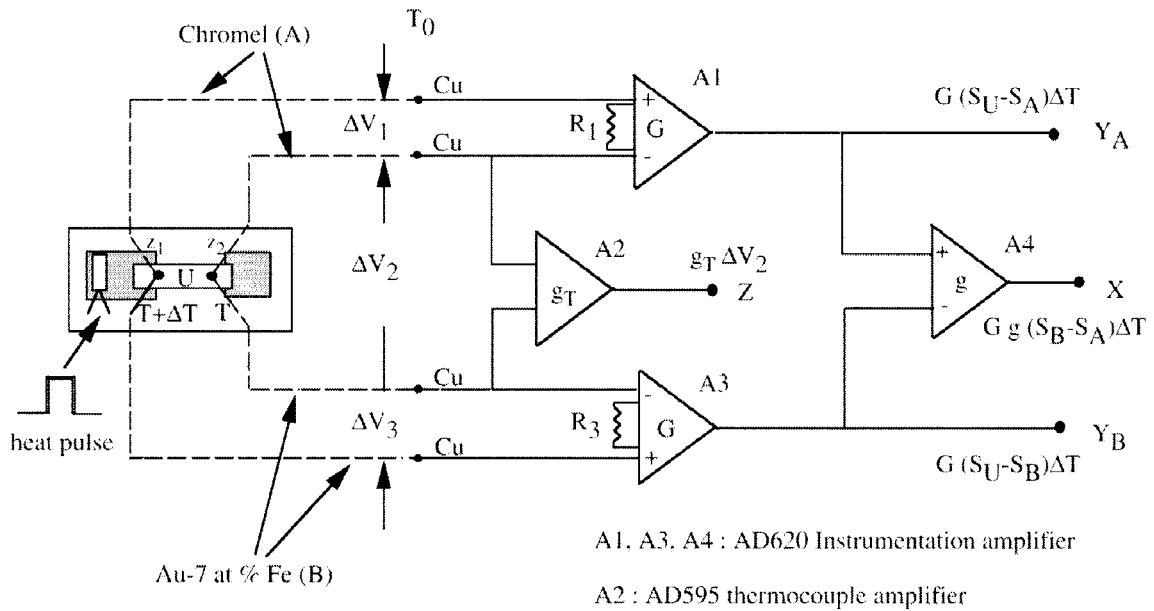


Fig 20: Figure of analogue subtraction circuit.

The pictures of apparatus used to measure in situ TEP and Resistance while introducing pH controlled gases are shown in the following page.

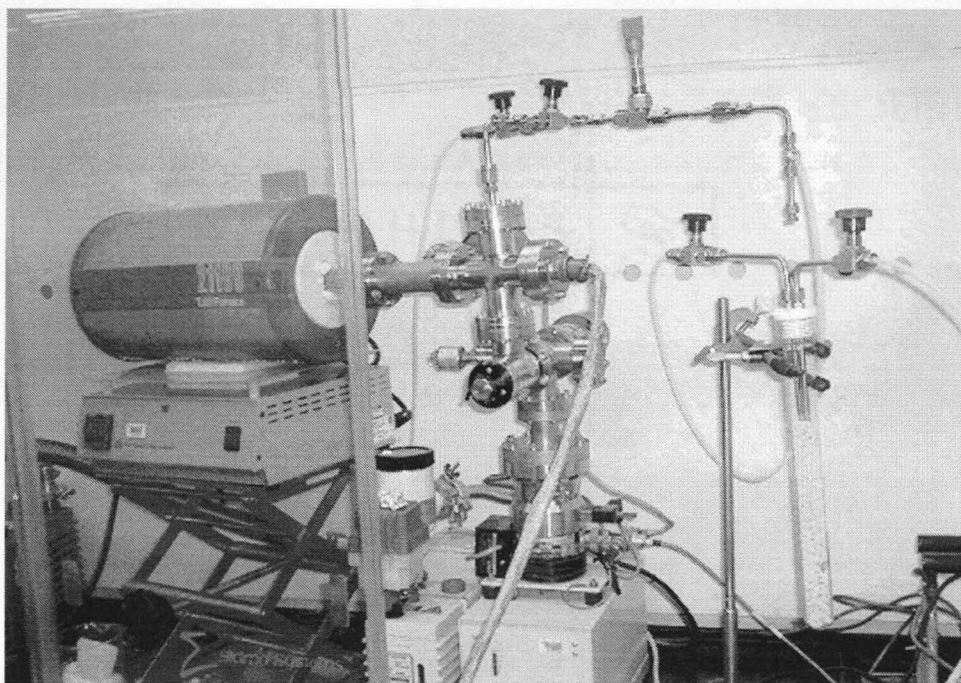


Fig 21: The Experimental Setup.

Mechanical pump allowed initial pumping to achieve a vacuum of a about 1 torr and the turbo molecular pump improved the vacuum down to about 1×10^{-6} Torr. To introduce different pH saturated gasses to the sample chamber, following bubbler setup was used

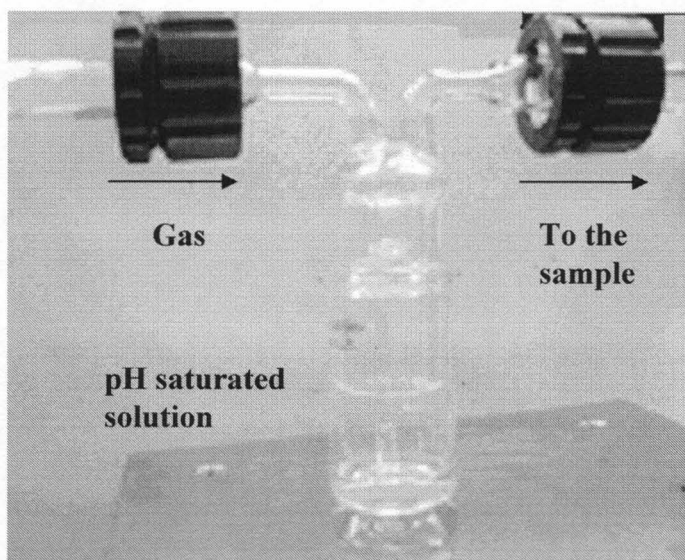


Fig 22: The bubbler setup used to introduce controlled pH solutions.

A moisture trap was utilized to minimize the water vapor, which allows dry gas in to the sample chamber. The moisture trap is a glass tube containing a mixture of CaCl_2 and CaO of dri-rite in which the inlet from the gas cylinder was connected. The outlet is connected to the sample chamber through a vacuum valve. The picture of the moisture trap is shown in the experimental setup.

Experimental Procedure

First the sample chamber and the connecting tubes were pumped using the turbo molecular pump. After turbo pump reached its maximum speed, the tube furnace was started by setting the temperature to 180°C at a ramping rate of 3-4deg/min. Once the furnace and pump are in operation, *in-situ* TEP and resistance measurements were obtained. During the heating of the sample under the vacuum, TEP was seen to slowly drop from a positive to a negative value [14]. When the desired TEP and vacuum level in the chamber were achieved by this degassing step, the furnace was turned off and allowed it to cool down to room temperature. Then at RT, gases with different pH values were introduced in to the sample chamber through glass bubbler of different pH solutions or moisture trap. Labview programs were used to collect the in situ TEP and resistance data separately. The following figures show the user interfaces of the labview programs.

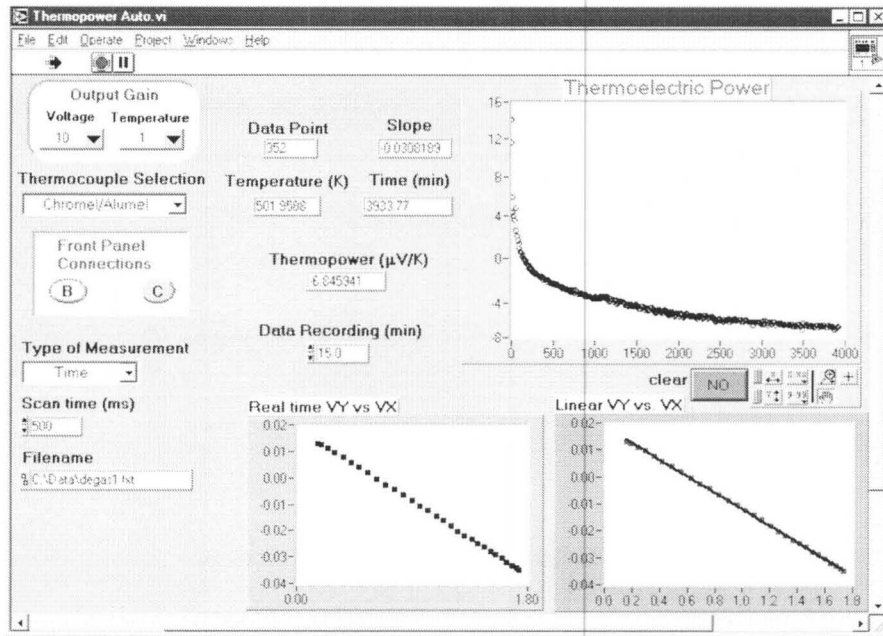


Fig 23: The user interface labview program used to collect thermoelectric power data for the thin film of SWNT.

CHAPTER 3: RESULTS & DISCUSSION

This chapter is mainly focused on the results and analysis on the single-walled carbon nanotube thin film samples. Several characterization techniques were employed to identify the type, structure and other behaviors of these samples. SEM, Raman and UV-VIS spectra are shown in the early sections. Then the chemical potential in a redox couple involving $O_2/H_2/H_2O$ is discussed. Finally, the electrochemical mediated charge transfer between the SWNT sample and aqueous solutions with different pH values were shown with TEP and 4-probe resistance measurements.

SEM images of SWNT Sample

The SEM images of the single-walled carbon nanotube thin films for purified and unpurified sample are shown in Fig 24

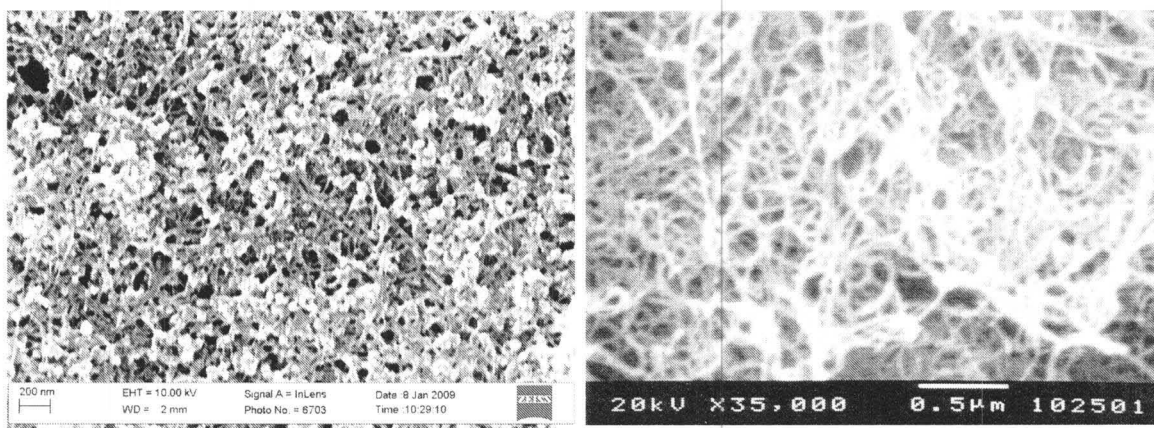


Fig 24: HRSEM images of purified & unpurified samples.

The observed impurities consist of amorphous carbon and other carbonaceous species and metals. The purified carbon nanotubes constitute of entangled ropes as an inter-twinned network.

The Raman Spectrum

The Raman spectrum of the single-walled carbon nanotube thin film was obtained using the Raman spectrometer for wavelength of 632.8nm. The spectrum is shown below.

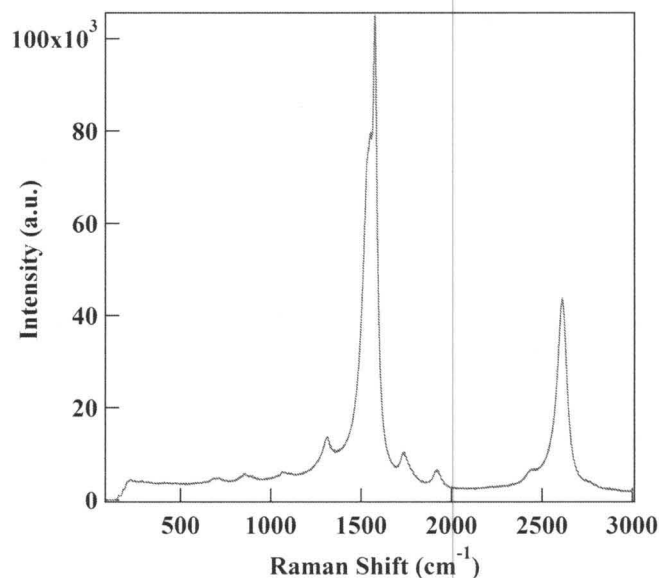


Fig 25: The Raman spectrum for the wavelength of 632.8nm.

The above spectrum shows a strong band $\sim 1584 \text{ cm}^{-1}$ which corresponds to the G band. Also there exists another peak $\sim 200 \text{ cm}^{-1}$ corresponding to the RBM mode. Presence of the RBM mode validates the presence of SWNTs. Since the laser with 632.8 nm can excite both metallic and semiconducting tubes (according to the Kataura plot) the Raman

confirms that the sample consists of a mixture of metallic and semiconducting single-walled carbon nanotubes.

The UV-VISIBLE-NIR Absorption Spectrum of SWNT thin film

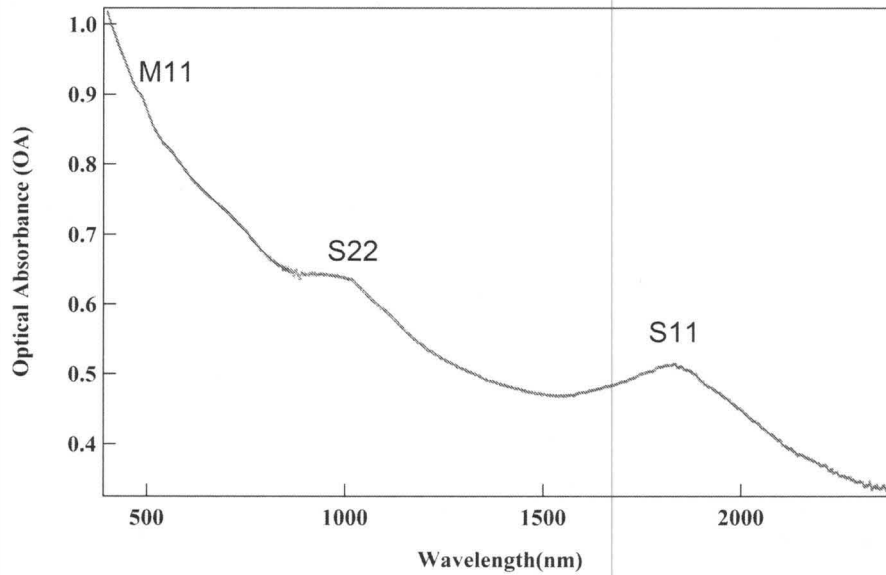


Fig 26: Optical Absorbance of the SWNT thin film obtained by the UV-IR spectrometer.

The optical absorbance of the thin film in the range 0-2500nm is shown in the graph above. The spectrum consists of sharp peaks corresponds to the first van Hove transitions of metallic swcnt (M_{11} =400-600nm), the first (S_{11} =800-1400nm) and second (S_{22} =550-800nm) van Hove transitions of semiconducting swcnts [21]. A spectrum from a bare glass substrate was useful as the reference beam. The spectrum covers UV-Visible-near-Infrared range giving peaks at 400, 1000 and 1800nm. The UV-VISIBLE spectrum of the sample after background subtraction is shown below.

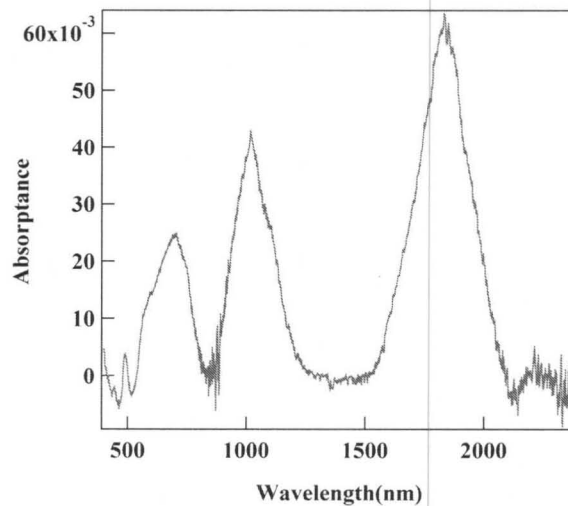


Fig 27: Background subtracted UV-VISIBLE-NEAR IR range absorption spectrum.

Chemical Potential and pH values of Aqueous Solutions

The relationship between the Electrochemical potential, pH value and Partial pressure of a gas is given by the Nearst equation [13]. The above equation is true for reactions occurred in acidic conditions.

$$\mu_e \text{ (eV)} = -4.44 + (-1)(1.229) + 0.0592/4 \times [4\text{pH} - \text{Log}_{10} (\text{P}(\text{O}_2)))] \text{ -----(1)A}$$



Reactions occurred in basic conditions.



$$\mu_e \text{ (eV)} = -4.44 + (-1)(0.401) - 0.0592/4 \times [4\text{pOH} + \text{Log}_{10} (\text{P}(\text{O}_2))] \text{ -----(2)A}$$

Here the partial pressure of O₂, P(O₂) is in bar. Also the electrochemical potential of electrons relative to the vacuum level is -4.44eV. The standard electrode potentials of the reactions of (1)B and (2)B are 1.229V and 0.401V versus Standard Hydrogen Electrode(SHE) respectively. Furthermore, pH + pOH = 14 [13].

For a given partial pressure of oxygen, say at 1bar (1 atm), the chemical potential variation as a function of pH value according to the equating (1)A is given below.

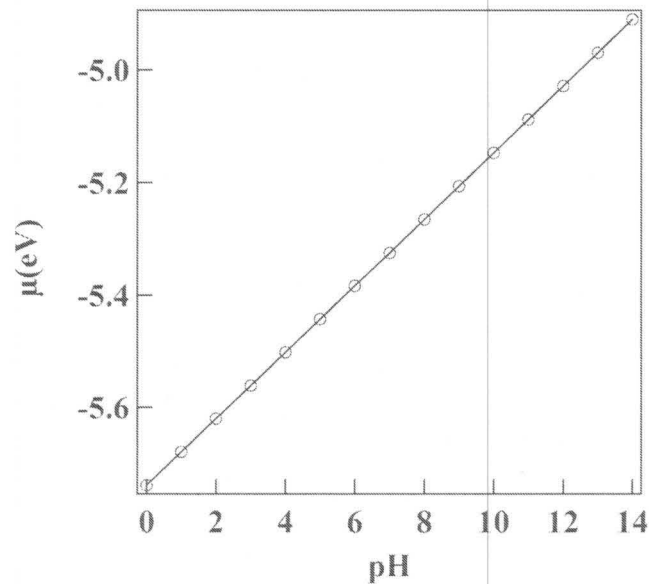


Fig 28: Graph of Chemical Potential as a function of pH value at Partial pressure of 1bar.

For a given pH value of 1.68, graphical representation of the Chemical potential as a function of Partial pressure of oxygen (P(O₂)) is shown below.

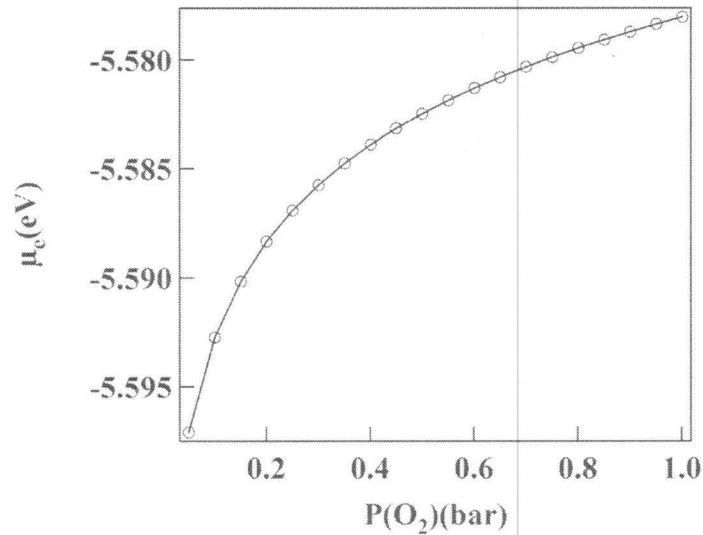


Fig 29 Graph of Chemical Potential as a function of Partial pressure of Oxygen at pH=1.68.

For water equilibrium with air, ie for pH=6:

$$\mu_e = -4.44 - 1.229 + (0.0592/4)(4 \times 6 - 0) = -5.31 \text{ eV by (1)A}$$

also by (1)A for partial pressure 1bar, which gives $\text{Log}_{10} [P(\text{O}_2)]=0$, the chemical potential for acidic condition will be:

$$\mu_e = -4.44 - 1.229 + (0.0592/4)(4 \times 1.68 - 0) = -5.57 \text{ eV}$$

Similarly, at the basic conditions the chemical potential will be:

$$\mu_e = -4.44 - 0.401 - (0.0592/4)(4 \times 12.45 - 0) = -5.58 \text{ eV}$$

Furthermore from the earlier work done by Chakrapani et. al., [13], the calculated values for chemical potential for acid of pH=0 and base of pH=14 are given by -5.65eV and -4.86eV respectively. The positions of the conduction and valence bands are known to be -4.8eV and -5.4eV respectively with an energy gap of about 0.6eV[16]. From above values, we can predict that the chemical potential of an acid of pH=0 lies below the

valence band and the Chemical potential of a base of $\text{pH}=14$ lies below the conduction band.

TEP and Resistance measurements on Electrochemical Charge transfer between the SWNT thin film and aqueous solutions

When the SWNT sample is degassed in a vacuum, the initial positive thermoelectric power gradually became negative [14], making it n-type thereby pushing the Fermi level towards the conduction band. The figure corresponding to degassing of the sample is shown below.

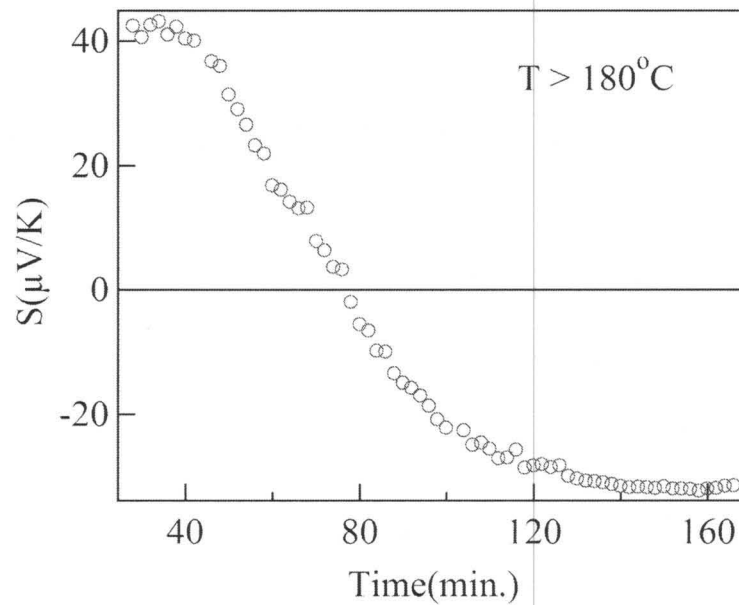


Fig 30: N-type conductivity of the sample under vacuum.

On the other hand, when air saturated with water vapor is introduced into the sample chamber, the thermoelectric power becomes positive again very rapidly. This air exposure effect dominated by oxygen making nanotubes p-type has been observed by

Zhao et. al[17]. Change of thermoelectric power from negative to positive upon exposure to air or oxygen[18] & [19] have also been observed by other groups. We also performed the thermoelectric power measurements for the same sample with gas containing vapor of different pH solutions. The negative thermoelectric power was always maintained at the same value ($S=-25\mu\text{V/K}$). The following graph shows the variation of thermoelectric power in response to different pH solutions. It is clear that for ambient conditions the thermoelectric power shows a higher change from negative to positive compared to dry oxygen for which the content was minimized using a moisture trap. This graph also shows that acidic vapor has the highest rate of change in the thermoelectric power.

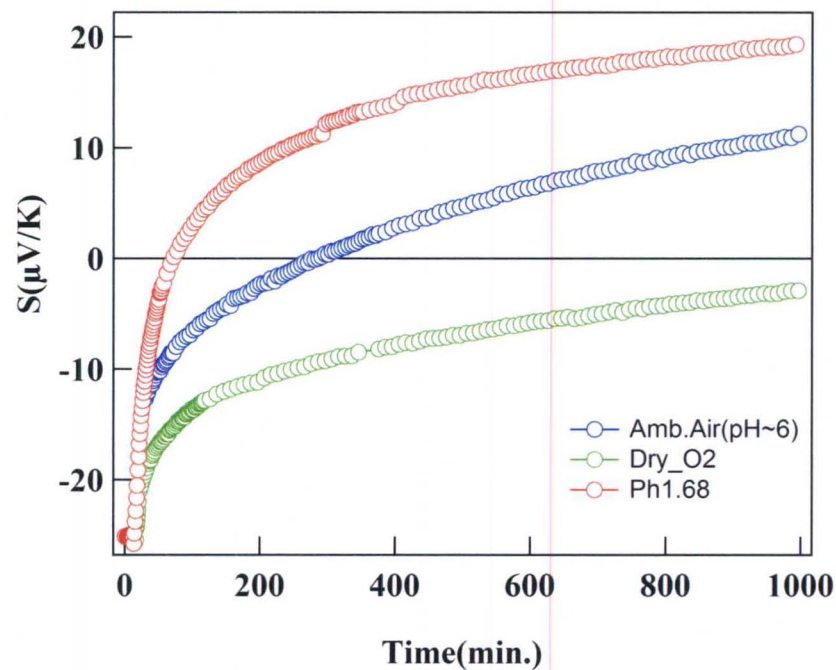


Fig 31: The Thermopower data exposed to oxygen through different pH values.

This observation is well described by the following mechanism.

The chemical potential of pH=1 acid is about -5.61eV according to the Nerst equation[13] and which is just below the conduction band. When the SWNT sample is n-type where the majority carriers are electrons, the charge (mostly electrons) may transfer from the carbon nanotube sample to the watery layer. This charge transfer depends on the positions of chemical potential of ambient layer and the Fermi-level of the nanotube. So larger the gap between Fermi-level and chemical potential, higher the charge transfer from nanotube to the ambient layer. The graph shows a higher rate of charge transfer for acidic solution than other situations. The next graph shows the corresponding resistance plot as a function of time similar conditions.

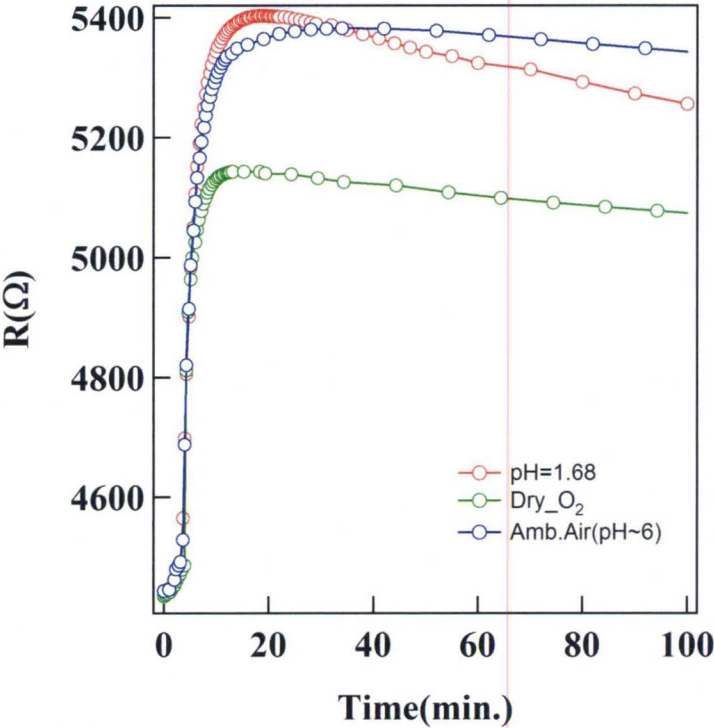


Fig 32: The Graph of Resistance against time for oxygen exposure to different pH values.

Again the resistance change is higher for pH=1.68 compared to other two.

The following graph shows the thermoelectric power and resistance as function of time of oxygen exposed to the sample through pH=1.68 acidic solution. Here the initial TEP value was maintained at two different values prior to the exposure.

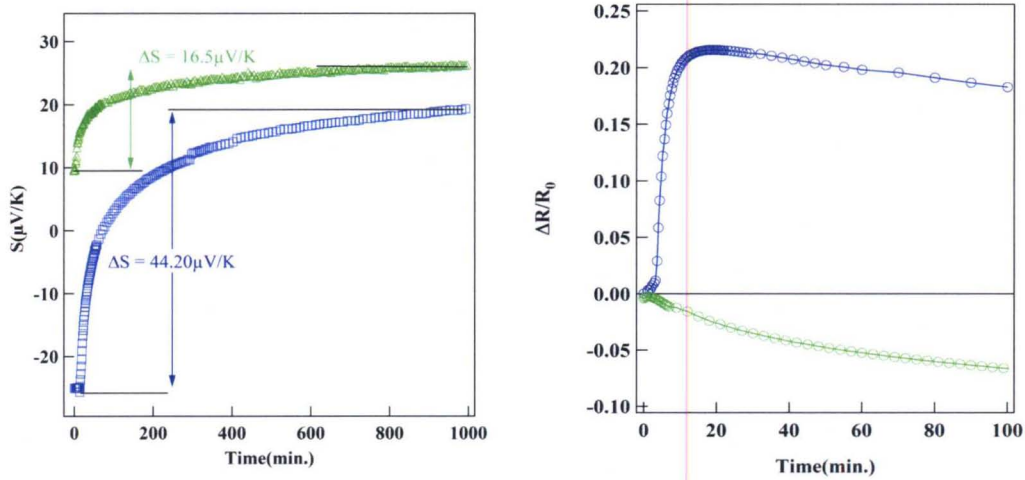


Fig 33: The Graphs of thermoelectric power and normalized resistance plotted as functions of time for $S=+10\mu\text{V/K}$ and $-25\mu\text{V/K}$ for the sample exposed to oxygen through an acidic solution of pH=1.68.

The change of thermoelectric power is higher for the initial positive $10\mu\text{V/K}$ (p-type) compared to that of $-25\mu\text{V/K}$ (n-type). But interestingly for n-type sample the resistance initially increased before it started to decrease after about 10minutes. Resistance of p-type sample decreases monotonically from the start. This behavior is explained using the following band-line diagram.

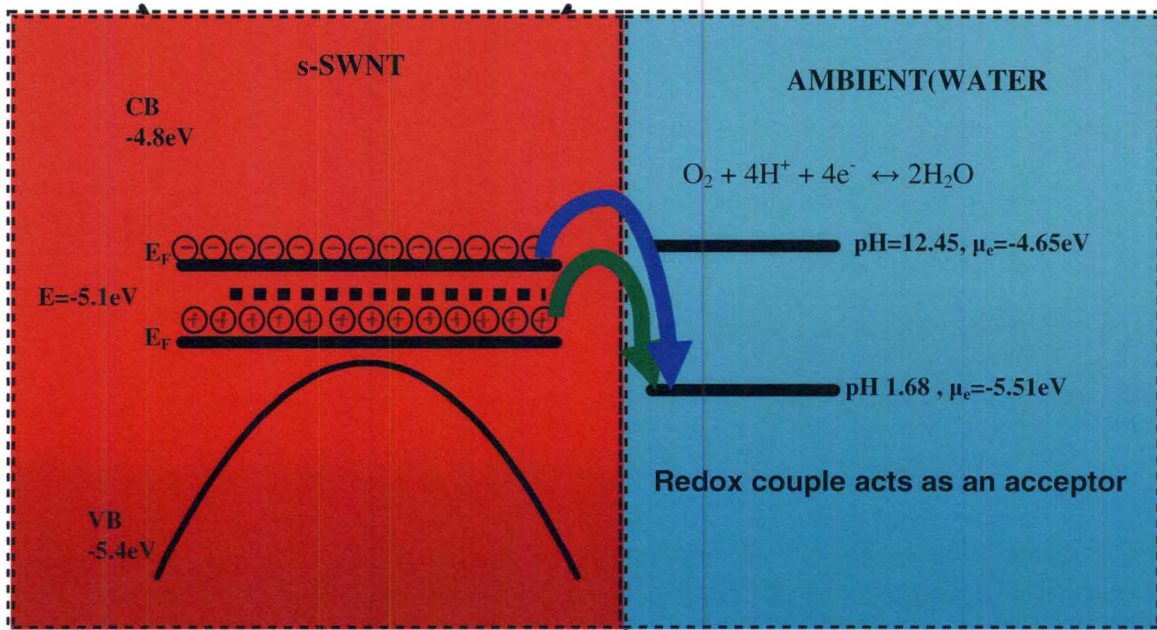


Fig 34: The Band line-up diagram for charge transfer between SWNT sample and an acidic solution of pH=1.68.

The separation between the Fermi-level of the nanotube and electrochemical redox couple in the ambient is related to the change of the thermopower. When the sample is n-type which has a negative thermopower, the Fermi-level lies closer to the conduction band. So the gap between the ambient layer and Fermi-level is higher compared to that for a p-type sample where the Fermi-level lies closer to the valence band. In both cases charge(electrons) is transferred from the nanotubes to the ambient layer because of the difference of the energy. In other words in this case the redox couple acts as an electron acceptor. For p-type sample where the holes are dominant, when the electrons are removed from SWNTs, the concentration of the holes become even more dominant pushing the Fermi-level towards the valence band. Thus the electrical conductivity increases resulting a decrease in the resistance. But when the sample is n-type where the electrons are dominant, further removal of electrons from the SWNTs pushes it towards valence band thus decreasing the conductivity of the sample. When it is closer to the

valence band again the removal of the electrons increases the hole concentration resulting an increase in the conductivity. This leads to a decrease of the resistance.

In the next experiment, the sample was exposed to oxygen through pH=12.45 under basic conditions. The following two graphs show the TEP and normalized resistance data for oxygen with pH=12.45.

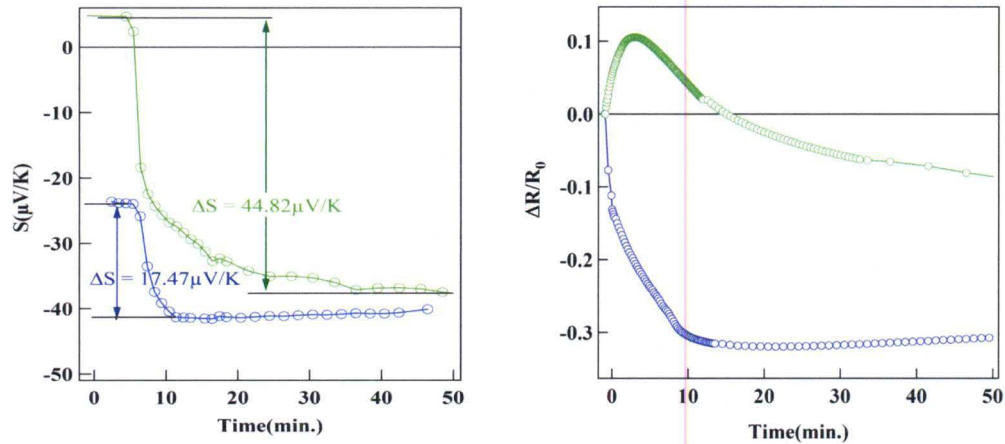


Fig 35: The Graphs of thermoelectric power and normalized resistance plotted as functions of time for $S=+10\mu\text{V/K}$ and $-25\mu\text{V/K}$ for the sample exposed to oxygen through a basic solution.

The thermopower and resistance data were obtained for two different initial values ($+10\mu\text{V/K}$ and $-25\mu\text{V/K}$). Again the thermopower data can be explained in relation to separation between the electrochemical potential of the ambient and Fermi-level of the SWNTs. The p-type sample shows a higher change in TEP compared to n-type sample. For the resistance, the p-type sample shows a peak while for n-type shows a clear monotonic drop of resistance. This is well related with the following band-line up diagram.

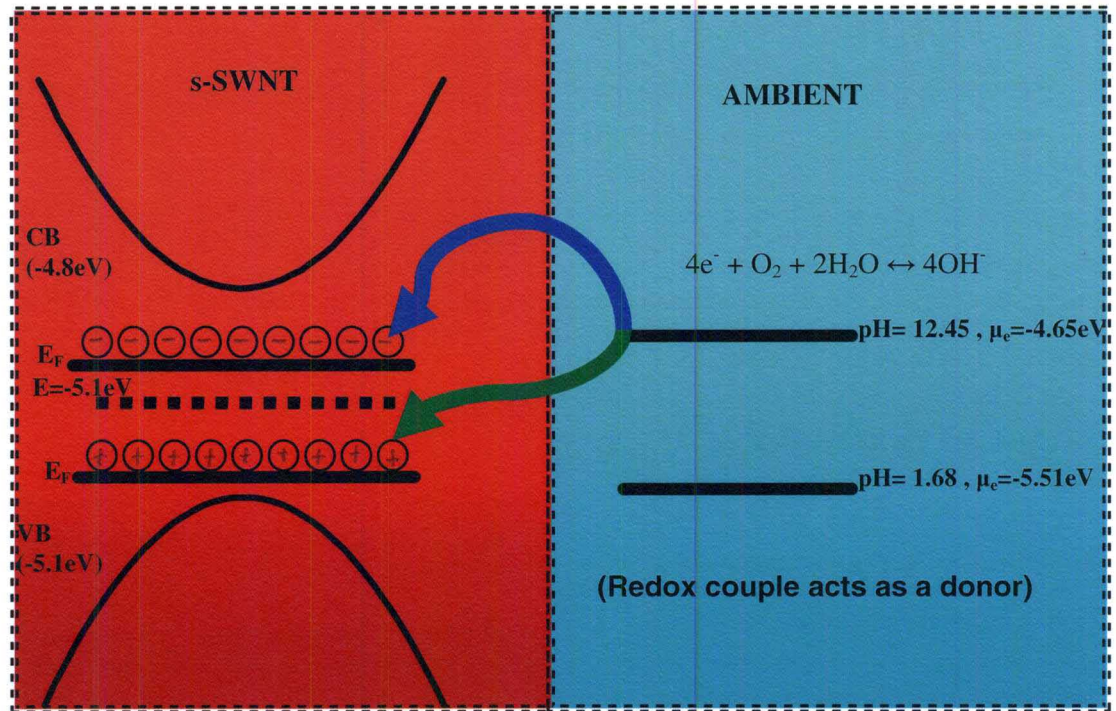


Fig 36: The Band line-up diagram for charge transfer between SWNT sample and a basic solution of $\text{pH} = 12.45$.

In this case the redox couple corresponds to $\text{pH} = 12.45$ lies above to that of $\text{pH} = 1.68$ according to the Nernst relationship. Again due to the misalignment of the chemical potential of $\text{pH} = 12.45$ and Fermi-level of the sample, a charge transfer takes place. In both cases the Fermi-level lies below the chemical potential of the ambient layer resulting a charge transfer from the redox couple to the nanotubes. Hence the redox couple in this case acts as an electron donor.

When the sample is n-type where the electrons are dominant, transfer of electrons from the ambient layer to the Fermi-level increase the number of electrons in the Fermi-level causes an increase in the electrical conductivity and hence decreasing the resistance. But when the sample is p-type, transfer of electrons to the sample depletes the electron

concentration in the sample pushing the Fermi-level towards the conduction band. Due to the depletion of holes, the conductivity decreases, resulting an increase in the resistance. When the Fermi-level is closer to the conduction band, the electron dominant environment increases the electron concentration by the charge transfer and decreases the resistance.

Finally the following figure shows the behavior of thermopower when exposed to hydrous ammonia.

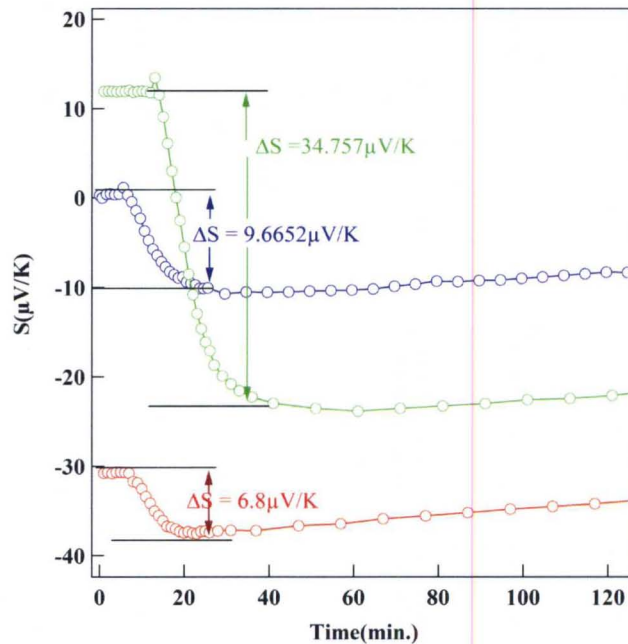


Fig 37: Graph of thermoelectric power as a function of time for hydrous ammonia exposure.

We clearly observed that the change of thermopower to be initially the higher for p-type sample compared to that of initially n-type sample indicating that the difference between the chemical potential corresponds to the redox couple and Fermi energy is higher for a p-type sample compared to n-type one. This is also well correlated with above

mechanism. This behavior of NH_3 molecules on nanotube is related with the results shown by Chang et. al in 2001[20].

CHAPTER 4: CONCLUSIONS

The *in-situ* thermoelectric power and 4-probe resistance were measured for thin films of semiconducting single-walled carbon nanotubes by exposing to gasses through under varying pH values. A Single-walled carbon nanotubes under ambient conditions show p-type conductivity, but upon degassing under high vacuum thermoelectric power gradually decreases and saturates with n-type conductivity. Also the presence of moist oxygen shows a much higher charge transfer compared to dry oxygen implying that moist oxygen is essential for the charge transfer to occur between the single-walled carbon nanotubes and the environment. The redox couple according to the Nernst equations corresponding to acidic solution acts as an electron acceptor from the single-walled carbon nanotubes which the redox couple corresponding to the basic solution acts as an electron donor to the nanotube.

Systematically shifting the Fermi-level by control removal of oxygen through the redox couple and exposing to moist oxygen explains the mechanism of the charge transfer occurred between the single-walled carbon nanotubes and ambient condition. We strongly believe that the same mechanism explains the charge transfer on other nano structures like multi-walled carbon nanotubes, Activated carbon fibers (ACF) and Graphene. Furthermore, this dramatic behavior upon gas exposure must be shown by individual single-walled carbon nanotubes which are much more sensitive than single-walled carbon nanotube bundles.

REFERENCES

1. Wildoer, J.W.G., Venema Liesbeth, C., Smalley, R. E., Dekker, C.,(1998) Electronic Structure of atomically resolved carbon nanotubes. *Letters of Nature*. Vol. 391, (59-61).
2. Jalilian, R.,(2004). Novel Synthesize Techniques for Nanostructures.
3. Saito, R., Dresselhaus, G., Dresselhaus, M.S., (1998). Physical Properties of carbon nanotubes.
4. Hugo, E.R.,(2004). Effects of Gas Interactions on the transport properties of single-walled carbon nanotubes.
5. Bhushan, B., (2004). Springer Handbook of Nanotechnology. (Chapter 13).
6. Jones, A.C., Hitchman, M.L.,(2009). Chemical Vapor Deposition; Precursors, Processes & Applications.
7. Meyyappan, M., (2005). Carbon Nanotubes ; Science & Applications.
8. Lamberti, C., (2008). Characterization of Semiconductor Hetrostructures and Nanostructres.
9. Dresselhaus, M.S., Dresselhaus, G., Saito, R., Jorio, A., (2004) Raman Spectroscopy of Nanotubes. Physics Reports.
10. Desai, S.C., Hewaparackrama, K. P., Jayasinghe, C., Mast, D., Pradhan, B, K., Sumansekara, G. U., (2008). Desorption Kinetmatics of Oxygen in Plasma treated

- SWNTs by *in situ* thermoelectric power measurements. *Nanotechnology*, Vol.19, 095507(1-5pp).
11. Rivera, J.E., (2004). Electrical Charge Distribution studies in SWNT, C60@SWNT & DWNT Structures.
 12. Sumanasekara, G. U., Grigorian, L., Eklund, P., (1999). Low-Temperature thermo electrical power measurements using analogue subtraction. *Meas. Sic. Technol.* Vol.11, 273-277.
 13. Chakrapani, V., Angus, John C., Anderson, Alfred B., Wolter, Scott D., Stoner, Brian R., Sumanasekera, Gamini U.,(2007). Charge Transfer Equilibria between Diamond and an Aqueous Oxygen Electrochemical Redox Couple. *Science*, Vol.318,1424-1430.
 14. Collins, P., Bradley, K., Ishigami, M., Zettli, A., (2000). Extreme oxygen sensitivity of Electronic properties of Carbon nanotubes. *Science*, Vol.287, 1801-1804.
 15. Tchernatinsky, A., Desai, S., Sumanasekara, G.U., Jayanthi, C.S., Wu, S.Y.,(2006). Adsorption of Oxygen molecules on individual single-wall carbon nanotubes. *Applied Physics*, Vol.99,034306-034310.
 16. Kazaoui, S., Minami, N., Matsuda, N., Kataura, H., Achiba, Y., (2001). Electrochemical tuning of electronic states in single-wall carbon nanotubes by in-situ absorption spectroscopy and ac resistance. *Applied Physics Letters*, Vol.78, 3435.
 17. Zhao, J., Buldum, A., Han, J., Lu, J., (2002). Gas molecule adsorption in Carbon nanotubes and nanotube bundles. *Nanotechnology*, Vol.13, 195-200.
 18. Bradley, K., Jhi, S., Collins, P., G., Hone, J., Cohen, M., L., Louie, S., G., Zettl, A., (2000). *Physical Review Letters*, Vol. 85, 4361-4364.
 19. Desai, S., C., (2004). Effect of Gas on Individual Single-walled Carbon nanotube Bundles.
 20. Chang, H., Lee, J., D., Lee, S., M., Lee, Y., H., (2001). Adsorption of NH₃ and NO₂ molecules on carbon nanotubes. *Applied Physics Letters*, Vol. 79, 3863-3865.
 21. Cao, C., Kim, J., H., Yoon, D., Hwang, E., Kim, Y., Baik, S., (2008). Optical detection of DNA hybridization using absorption spectra of single-walled carbon nanotubes. *Materials Chemistry and Physics*, Vol. 112, 738-741.

CURRICULUM VITAE

NAME: Buddika KA Abeyweera MP.

ADDRESS: Department of Physics & Astronomy
102 Natural Science Building
University of Louisville
Louisville, KY 40292.

DOB: July 23, 1980.

EDUCATION: M.S., Physics
University of Louisville
Louisville, KY 40292.
2007-2009

PROFESSIONAL SOCIETIES:

Member of the American Physical Society.

NATIONAL MEETING PRESENTATIONS:

“Transport Properties of Carbon nanotubes” American Physical Society March Meeting 2009, Pittsburgh.

BOOKS AND SYMPOSIA:

Poster Presentation in Electrochemically mediated charge transfer effects on SWNTs. Graduate Symposium, March 2009. University of Louisville.